Calspan

Technical Report

FINAL SUMMARY REPORT

APRIL 1969 – JUNE 1974

CONTRACT NO. NAS 8 24072

Prepared for:

GEORGE C. MARSHALL SPACE FLIGHT CENTER
NATIONAL AERONAUTICS AND SPACE ADMINISTRATION
HUNTSVILLE, ALABAMA

Calspan Corporation
Buffalo, New York 14221

Formerly Cornell Aeronautical Laboratory, Inc.

Calspan

AERODYNAMIC AND BASE HEATING STUDIES ON SPACE SHUTTLE CONFIGURATIONS

By: K.C. Hendershot and R.J. Vidal

Calspan Report No. AA-2793-Y-2
November 1974

FINAL SUMMARY REPORT

APRIL 1969 – JUNE 1974
CONTRACT NO. NAS 8 24072

BY: K. C. Hendershot
K.C. Hendershot

APPROVED: A. Ritter
A. Ritter, Assistant Head
Aerodynamic Research Department

R. J. Vidal
R.J. Vidal

Calspan Corporation
Buffalo, New York 14221

FOREWORD

The research effort reported herein was performed for the Marshall Space Flight Center of NASA under Contract NAS8-24072. Technical direction was provided by Messrs. Homer Wilson, Jr. and David Seymour of the MSFC.

SUMMARY

This report summarizes the results of two independent investigations performed by Calspan in support of NASA/MSFC Space Shuttle studies. One effort involved experimental measurements of the thermal environment in the base region of a Space Shuttle orbiter model at high altitudes. The second effort consisted of an analytical study of leeside heating effects on Space Shuttle-type bodies at hypersonic flow conditions.

The first section of this report describes the short-duration firing 4%-scale hot-flow rocket model employed for these measurements and presents experimental heating rate data obtained at simulated altitudes to 240,000 feet. The results of the leeside heating analysis, which is based primarily on correlations of experimental heating rate data previously collected in the Calspan hypersonic shock tunnels, are presented in the second section of the report.

TABLE OF CONTENTS

INTRODUCTION

As originally conceived in 1969, effort on this program was to be directed toward the acquisition of experimental data relating to the rarefied flow regimes of high altitude plumes in support of analytical studies which were in progress at MSFC. However, as the NASA study efforts on the Space Shuttle progressed during the early 1970's, it became apparent that base heating problems similar to those encountered on the Saturn family of boosters would have to be solved during the Space Shuttle development. As a result, in late 1970, Calspan's effort was reoriented toward the study of flow recirculation and base heating problems on clustered rocket configurations of the type being considered at that time for the Space Shuttle. A specific objective of that effort was an evaluation of techniques for achieving in base heating models the high combustion pressures (3000 psia) being employed for the full-scale Space Shuttle booster rocket engines.

In the spring of 1971, program objectives were further modified in scope to "provide experimental data on rocket exhaust flow fields from both single and clustered rocket nozzles at high altitudes and to investigate aerodynamic heating effects on the lee surface of various hypersonic configurations". Effort on the leeside heating effects on Shuttle-type configurations was satisfactorily completed and reported in early 1972. At the request of the NASA/MSFC Technical Monitor, technical activities on the task related to base heating effects on Space Shuttle-type geometries were purposely maintained at a low level until mid-1972 pending selection of the specific full scale Space Shuttle configuration to be developed by NASA.

In late summer of 1972, conceptual layouts of Space Shuttle base heating model designs were initiated by Calspan in preparation for future model base heating test programs. This effort continued until November 1972 at which time prime responsibility for the design and construction of a 4% scale orbiter base heating model was transferred to Grumman Aerospace Corporation (GAC) under a Rockwell International (RI) subcontract. Grumman, in turn, subcontracted with Calspan to perform the detail design and fabrication, following closely and integrating many of the concepts originally developed under the present program. At that time, the remaining funds on this contract were set aside to be used later to obtain preliminary base heating data during the checkout tests of the RI/GAC model, scheduled for mid-1973. Because of development problems with the model, however, these tests were delayed until December 1973, at which time a limited amount of base heating and pressure data was obtained at altitude conditions.

This report summarizes the findings of the two major tasks undertaken during the performance of this contract; i.e., base heating studies on the Space Shuttle orbiter configuration and analysis of leeside heating effects on Space Shuttle orbiter-type bodies. The results of these studies are presented as separate sections of this report.

Results of the other efforts performed during the course of this program, namely, (1) evaluation of high pressure model combustor techniques and (2) preliminary conceptual designs of Space Shuttle base heating model configurations, have been incorporated directly into the successful RI 19-OTS and 25-O base heating model designs and will not be reported here.

 N75 20449

A PRESENTATION OF BASE HEATING DATA OBTAINED FROM THE 25-O SPACE SHUTTLE MODEL AT HIGH ALTITUDE

K.C. Hendershot

Introduction

During Calspan's development of the 25-O Space Shuttle model for Grumman/Rockwell International, several test firings were made in a vacuum chamber at simulated altitude conditions in order to verify satisfactory ignition and operation of the model in a high altitude environment. In conjunction with these firings, heating rate pressure and measurements were obtained at several locations in the orbiter base region on a "piggy-back" basis, in support of the present program. This document presents a summary of the data obtained during these experiments and a brief description of the 25-O Space Shuttle model employed.

Test Model

The model used for these experiments is shown in cross-section in Figure 1 and consists of a hot-firing 4% scale model of the aft end of the Space Shuttle orbiter configuration. Included in the model configuration are the outer fuselage contour, the base region (including the three SSME's* and OMS* engines), OMS pods, the vertical fin, and the body flap. A complete model description may be found in Reference 1.

Combustor Assembly

The combustion system consists of three separate combustion chambers, each with its own 8-element triplet (2 oxygen impinging on 1 hydrogen) propellant injector. Propellants are routed to each injector via symmetrical manifolds. Pressure balancing between the three individual combustion chambers is provided by three ducts connecting to a small "collector" chamber located at the center of the combustor triangle. This collector chamber also

*SSME = Space Shuttle Main Engine
OMS = Orbit Maneuver System

contains the ignition source (a conventional spark plug) and two ducts which direct combusted gases to the OMS nozzles when they are used.

The high pressure gaseous oxygen and hydrogen propellants are stored in long charge tubes attached to the forward end of the model. Flow to the propellant injectors is initiated by the mechanical cutting of mylar diaphragms located at the downstream end of the storage tubes. Metering of the H_2 and O_2 flows for O/F and total mass flow control is provided by calibrated choked venturis located downstream of the diaphragms. Venturi inlet and combustion chamber pressures are measured for each run.

Model Base Configuration

The model base housing (which includes the heat shield and OMS pods) closely duplicates the orbiter external lines aft of Station 1400. The complete base assembly is seismically suspended from the combustor housing for shock isolation. Cutouts in the heat shield provide necessary clearance between the SSME and OMS nozzles and the metric base assembly. Foam rubber seals around the nozzles prevent gas leakage forward of the heat shield.

Although the heat shield was more thoroughly instrumented for the OH-8 test program subsequently performed at MSFC-IBFF (Reference 2), a limited number of sensors was installed for the present program at locations of interest to the MSFC technical monitor as shown by the solid symbols in Figure 2. It is observed that gages were primarily installed on the heat shield surface along a vertical ray between the two bottom engines, at several locations on an OMS pod, and on the body flap.

Data Acquisition

Model heating rates were measured with fast response thin-film heat transfer gages of the type employed by Calspan and other groups for many years for shock tunnel and base heating studies. The gages (described in detail in Reference 3) operate on the principle of transient heating of a semi-infinite slab of known thermal properties.

Base pressures were measured at two locations by means of Calspan-developed piezoelectric pressure transducers.

Data were recorded on oscilloscopes equipped with Polaroid cameras. Thin-film heating gage outputs were processed in real time by an analog network (Q-meter) to convert the temperature-time history to a signal directly proportional to heating rate prior to display on the oscilloscope.

Test Facility

The model was installed in the hatch opening of the Calspan 10-foot diameter x 28-foot long high altitude chamber. Pressures to $\approx$0.1 microns HgA are attainable in this chamber by use of a diffusion pump, although the present tests employed only the mechanical vacuum pumps. The 28-foot tank length provides a test duration of $\approx$10-12 msec as indicated by blast wave return at the model base.

Present Experiments

Test Conditions

A total of four test firings were made during which base data were collected. Ambient pressure in the altitude chamber varied from approximately 1 mm to 38 microns HgA. Combustion pressure of the SSME's ranged from 400 to 1000 psia, with corresponding OMS nozzle pressures of 40 to 100 psia. Model operating parameters are tabulated along with the base heating rate data.

Experimental Results

Reduced data from the four test runs are presented in Table I; corresponding raw data records and associated run logs are reproduced in Appendix A.

Since a large amount of data similar to that obtained during the present test series has subsequently been obtained at the NASA/MSFC-IBFF and analyzed in depth in Reference 2, a detailed presentation of the limited experimental results obtained during the present study is not warranted and will not be attempted here.

References

1. Herrera, B., "Pretest Information for Test (OH-8) of the 0.04-Scale Space Shuttle Orbiter Base Heating Model 25-O in the MSFC-IBFF", Rockwell International Report SD73-SH-0239, September 1973.

2. Seymour, D.C., "Analysis of OH-8 Orbiter Base Heating Data", MSFC Memorandum ED34-74-6, August 1974.

3. Bogdan, L., "Instrumentation Techniques for Short-Duration Test Facilities", Calspan Report WTH-030, March 1967.

TABLE I - REDUCED DATA FOR 25-0 MODEL C/O TESTS

SENSOR NUMBER	RUN 112 P_c = 400 PSIA. ALT = 150,000 FT.		RUN 113 P_c = 615 PSIA ALT = 210,000 FT.		RUN 114 P_c = 1060 PSIA ALT = 230,000 FT.		RUN 115 P_c = 1060 PSIA ALT = 210,000 FT.		NOTES
Q46	≈ 0	BTU/FT²-SEC	0.38	BTU/FT²-SEC	0.40	BTU/FT²-SEC	0.75	BTU/FT²-SEC	1. ALL NOZZLES IN NULL POSITION
Q53	↓	↓	0.24	↓	0.39	↓	0.52	↓	
Q54			—		—		—		2. THROAT DIAPHRAGMS EMPLOYED FOR ALL NOZZLES ON ALL RUNS
Q59			—		1.20		1.89		
Q64			>1.6		2.05		2.91		
Q66			0.99		2.18		—		3. NOMINAL O/F = 6.0
Q70			0.58		1.09		1.28		
QR92			<.007		<.003		.04		4. INDICATED $\eta_{c^*} \approx 80\%$ FOR ALL RUNS.
Q78			0.36		0.58		0.50		
Q87			0.06		0.06		0.08		5. NO O_2 LEAD
Q89			0.17		0.34		0.27		6. NO BURNING IN O_2 PASSAGES OBSERVED.
Q91			0.06		0.14		0.13		
Q92			0.36		0.53		>0.83		
Q95			0.41		0.64		0.62		
Q97			0.34		0.46		0.49		
Q101			0.53		0.27		0.29		
Q107			0.32		0.79		0.54		
Q109	↓	↓	—	↓	—	↓		↓	
P_c(OMS 1)	36	PSIA.	32	PSIA	—	PSIA	94	PSIA	
P30	—	↓	0.011	↓	—	↓	0.016	↓	
P32	—		0.016		.042		—		
P_c(SSME 1)	315		480		1090		810		
P_{NE}^*(SSME 1)	0.70		—		—		1.28		
P_{NE}(SSME 2)	0.71		1.06		2.27		2.01		
P_{NE}(SSME 3)	—		1.28		2.40		2.48		
P_{NE}(OMS 1)	—	↓	0.15	↓	0.34	↓	0.26	↓	

P_{NE} = NOZZLE EXIT PRESSURE

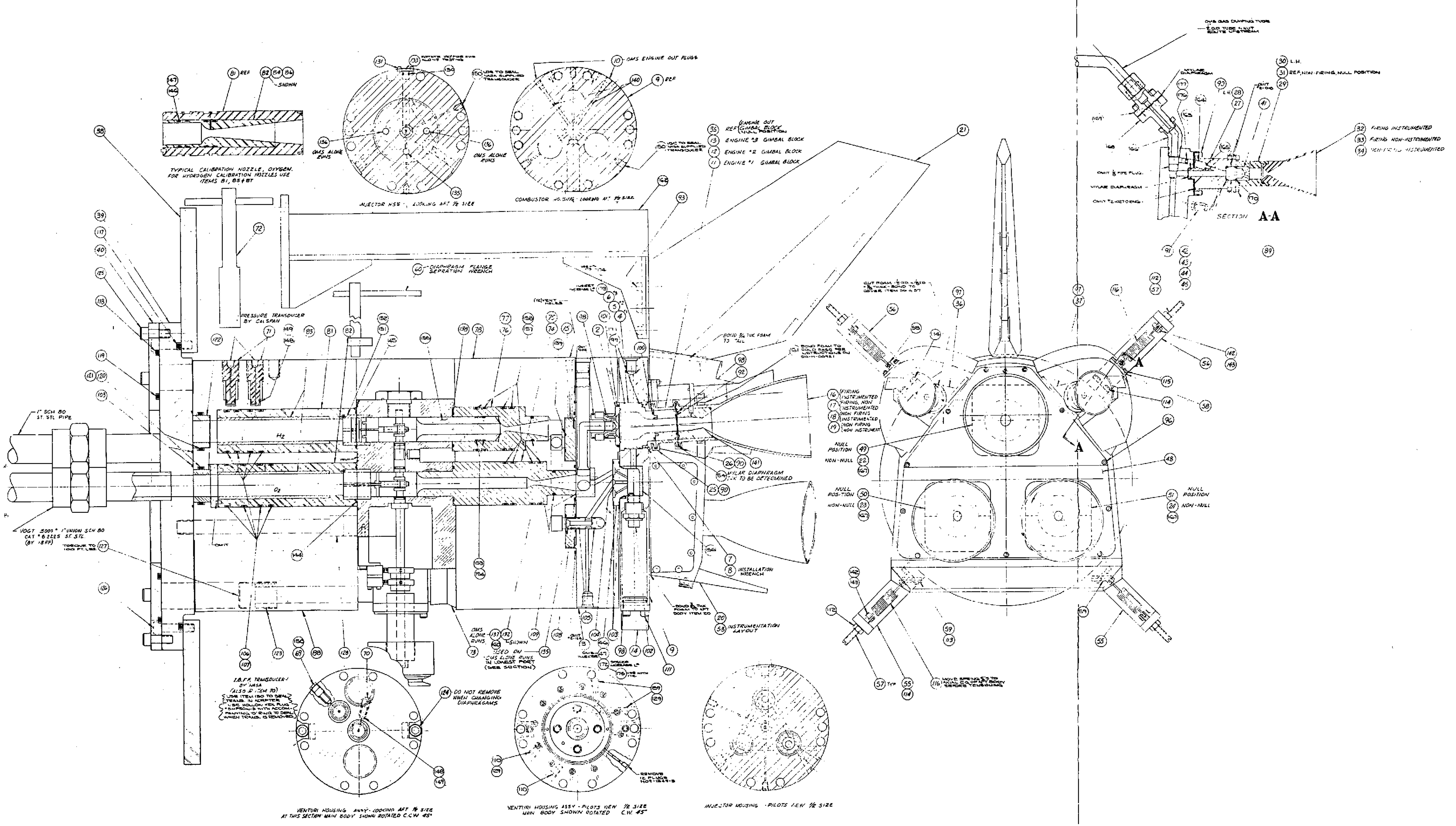

Figure 1 25-O MODEL CROSS-SECTION VIEW

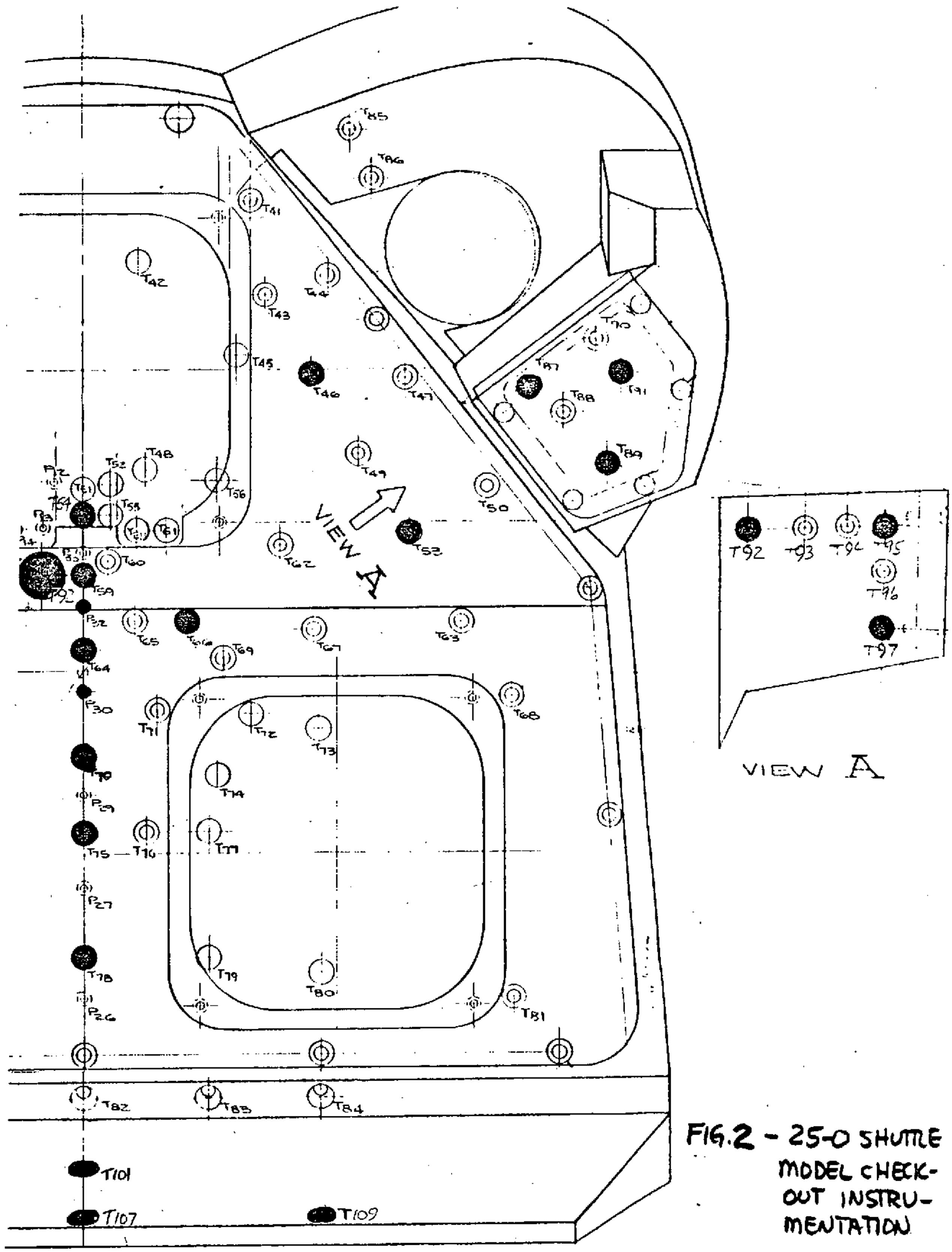

FIG.2 - 25-0 SHUTTLE MODEL CHECK-OUT INSTRUMENTATION

APPENDIX A

Original data logs and oscilloscope records for Runs 112, 113, 114, and 115 obtained during 25-O model combustor checkout tests are presented in the following pages.

$\overline{P}_{C(SSME)}$ = 400 PSIA ; $\overline{P}_{C(OMS)}$ = 40 PSIA.

ALT = 150,000 FT (1 mm Hg)

RUN 112

SCOPE CHANNEL	SENSOR	K(Ω/psi)	PRE-RUN R (Ω)	D.L.R. (KΩ)	SWEEP (MSEC/CM)
1	Q46	0.134	120	80 KΩ	5
2	Q53	0.125	102	160	
3	Q54	0.139	110	200	
4	Q59	0.115	92	40	
5	Q64	0.121	97	200	
6	Q66	0.135	106	80	
7	Q70	0.113	97	40	
~~8~~	~~Q84~~	~~0.142~~			
9	Q78	0.099	87	160	
10					
31	Q87	0.133	105	40	
32	Q89	0.139	130	80	
33	Q91	0.121	103	160	
34	Q92	0.096	84	80	
35	Q95	0.102	130	40	
36	Q97	0.096	88	160	
37	Q101	0.158	124	80	
38	Q107	0.140	111	80	
39	T109	0.127	30(?)	160	
40	Pc (OMS)	22.7 *	—	400 mV/CM	
41	P30	1741 *	—	10	
42	P32	1603 *	—	10	
43	Pc (SSME 1)	1.925 *	—	200	
44	PNE (SSME #1)	154 *	—	50	
45	PNE (SSME #2)	215 *	—	50	
46	PNE (SSME #3)	225 *	—	200	
47	PNE (OMS 1)	371 *	—	10	

* MV/PSI.

CALSPAN CORPORATION

Aerodynamic Research Department

1

Program 25 "0"

W. A. ______ Date 12-10-73 Run 112

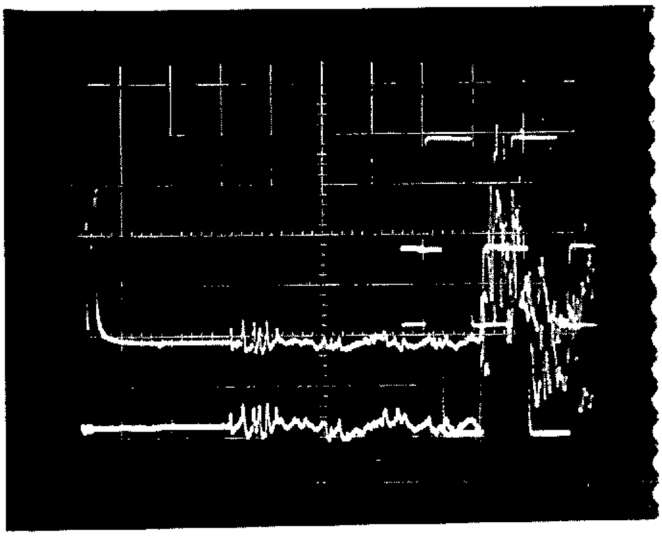

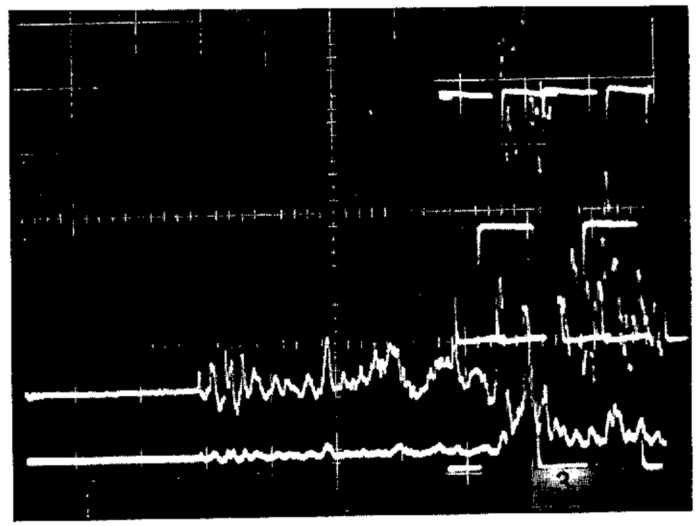

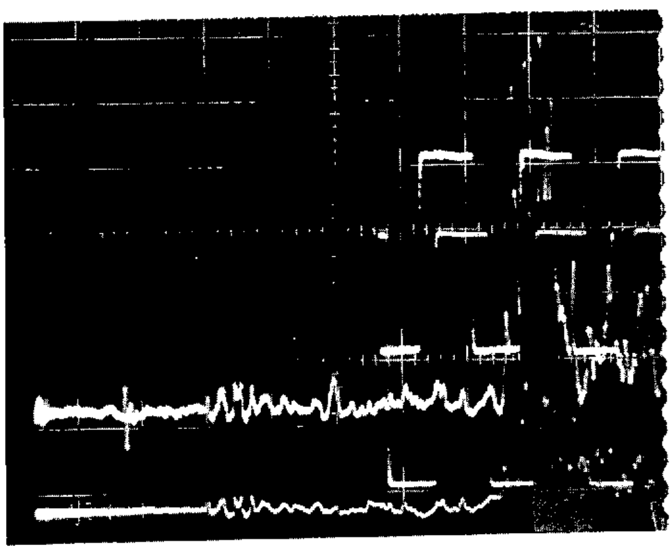

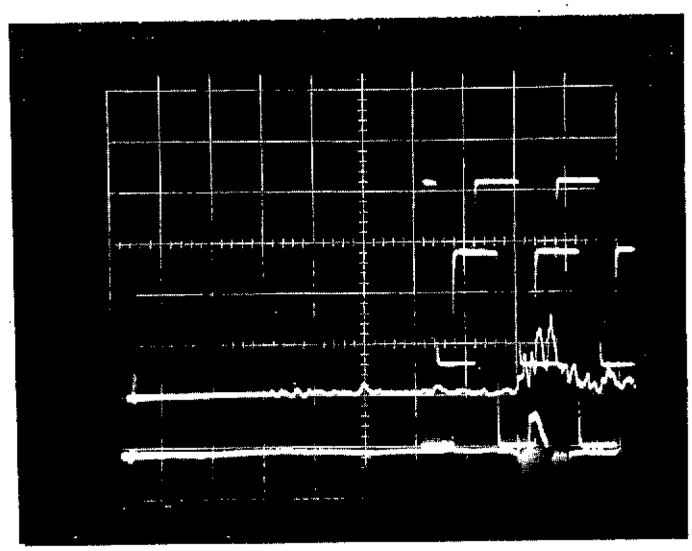

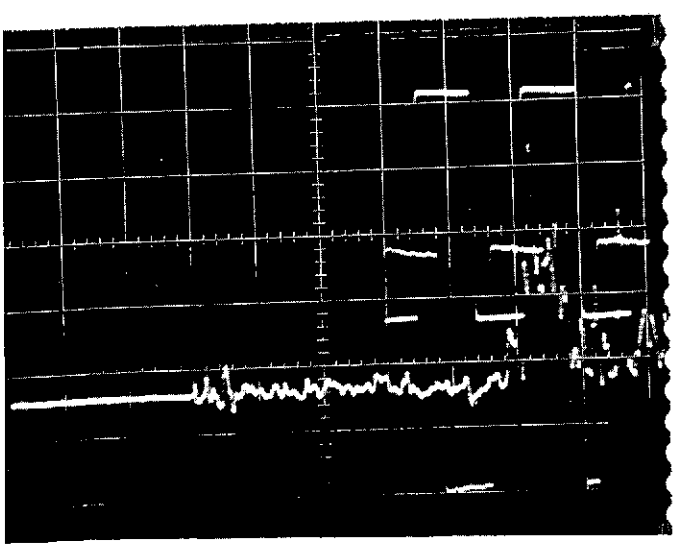

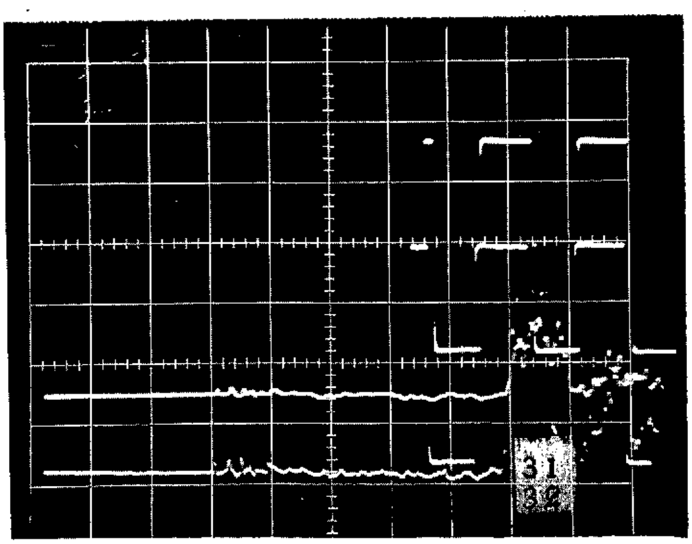

2

CALSPAN CORPORATION

Aerodynamic Research Department

Program 25 "0"

W. A. ________ Date 12-10-73 Run 112

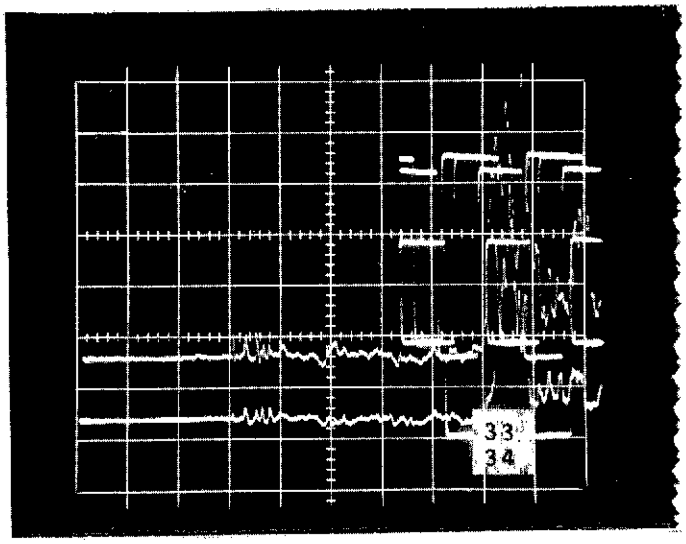

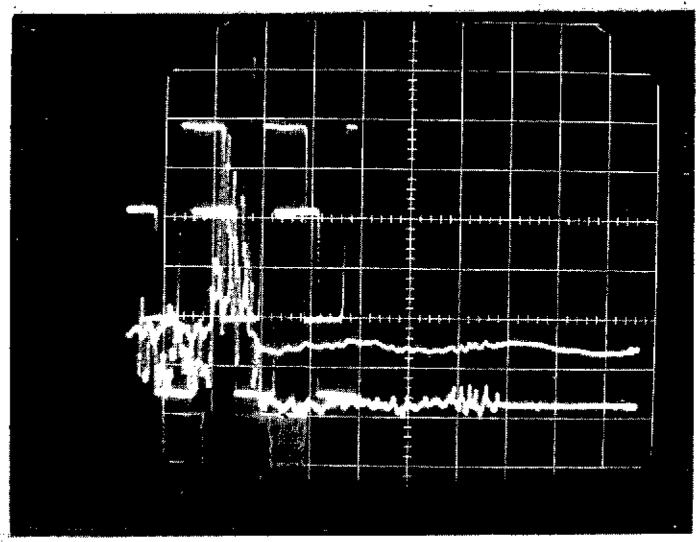

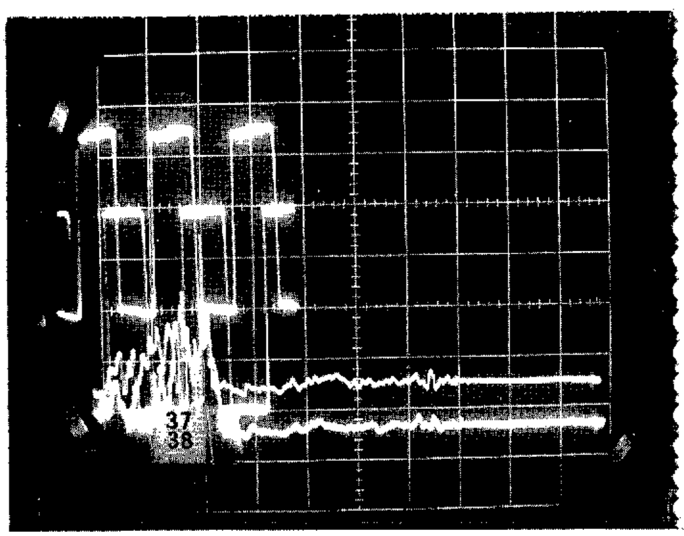

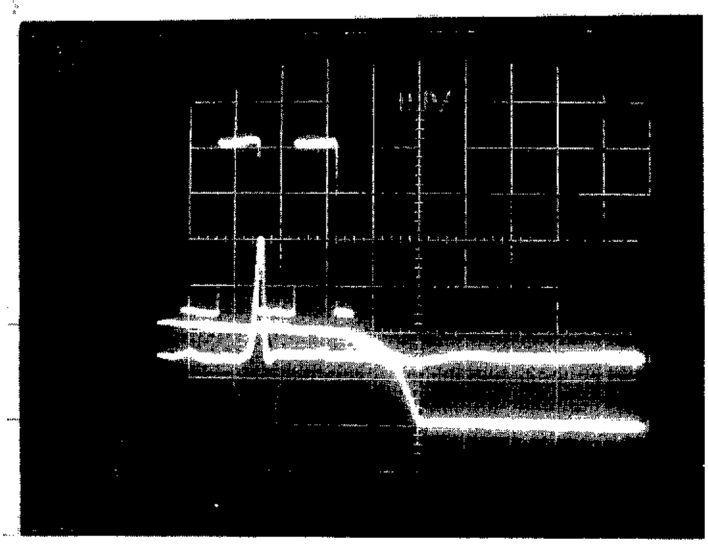

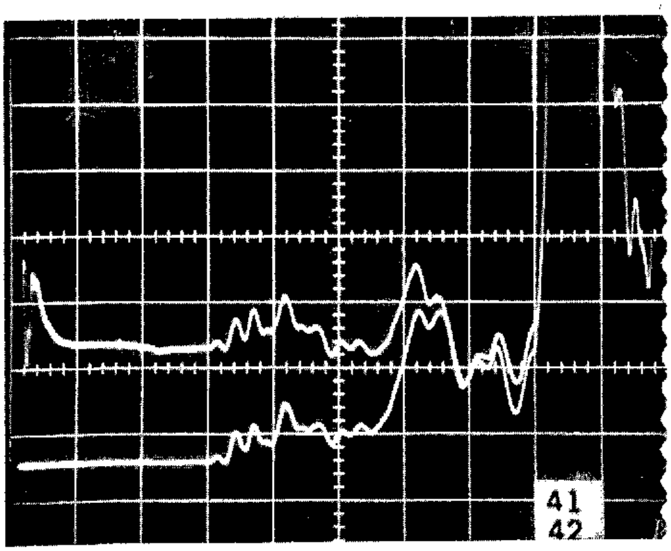

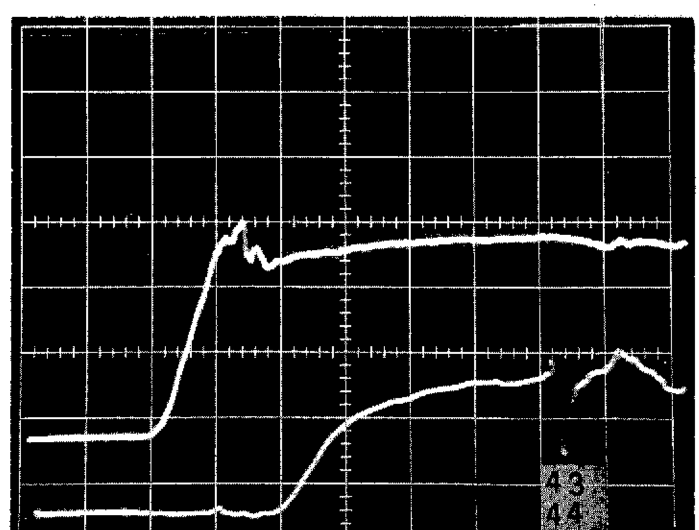

CALSPAN CORPORATION
Aerodynamic Research Department

(3)

Program 25 "0"
W. A. ______ Date 12-10-73 Run 112

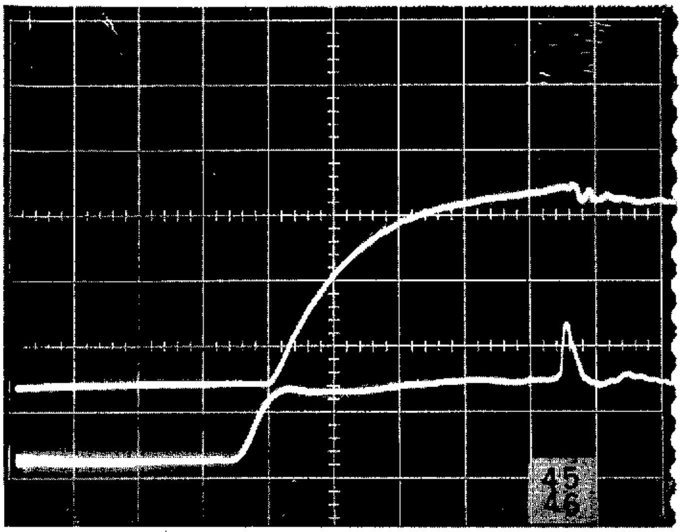

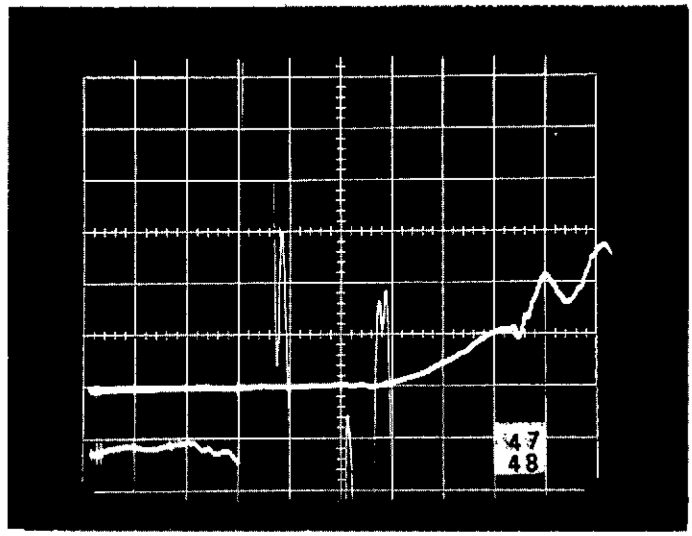

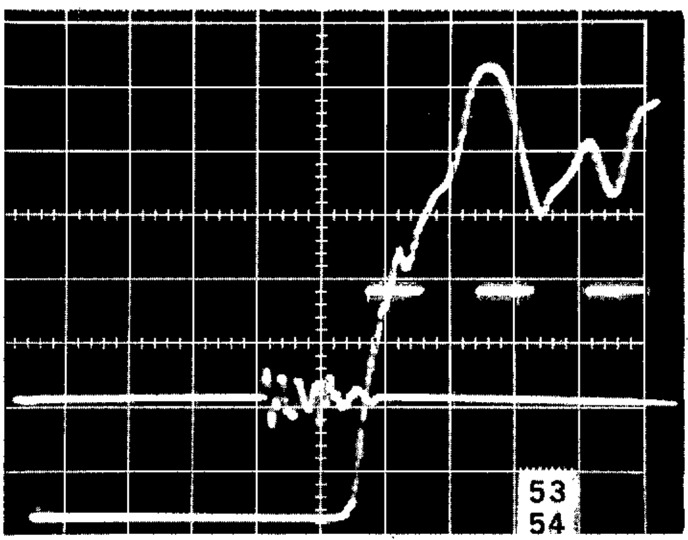

$\overline{P}_{c(SSME)} = 615$ PSIA ; $\overline{P}_{c\,(OMS)} = 58$ PSIA.
ALT = 210,000 FT. (100 μ)

RUN 113

SCOPE CHANNEL	SENSOR	K (Ω/°F.)	FREE-RUN R (Ω)	DLR (K-Ω)	SWEEP ([illegible]/CM)
1	Q46	0.134	106	200	5
2	Q53	0.125	103	100	
3	Q54	0.139	110	100	
4	Q59	0.115	94	200	
5	Q64	0.121	97	50	
6	Q66	0.135	107	20	
7	Q70	0.113	99	100	
8	QR92	0.142	103	200	
9	Q79	0.099	86	100	
10					
31	Q87	0.133	106	80	
32	Q89	0.134	112	200	
33	Q91	0.121	104	100	
34	Q92	0.096	85	100	
35	Q95	0.102	94	40	
36	Q97	0.096	90	100	
37	Q101	0.158	125	100	
38	Q107	0.140	110	100	
39	Q109	0.127	OPEN	—	
40	Pc (OMS 1)	22.7*		400 MV/CM	
41	P30	1741*		10	
42	P32	1603*		10	
43	Pc (SSME 1)	1.925*		800	
44	PNE ([illegible])	154*		50	
45	PNE ([illegible])	215*		100	
46	PNE ([illegible] #3)	225*		200	
47	PNE (OMS 1)	371*		10	

* MV/PSI.

CALSPAN CORPORATION

Aerodynamic Research Department

1

Program 25 "0"

W. A. ________ Date 12-10-73 Run 113

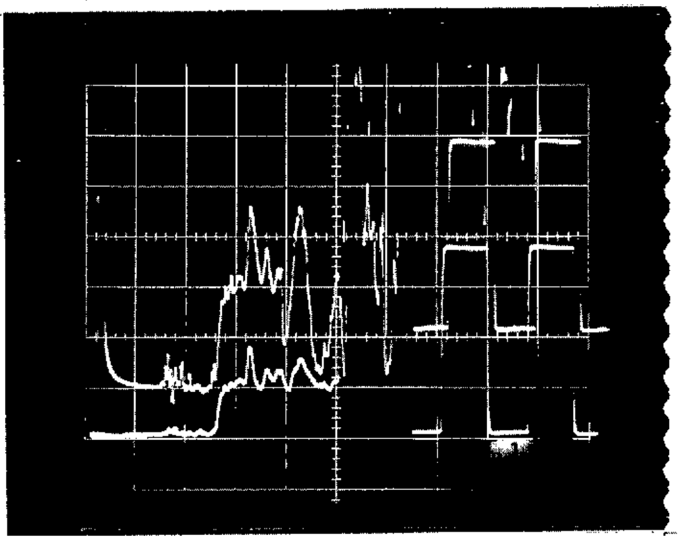

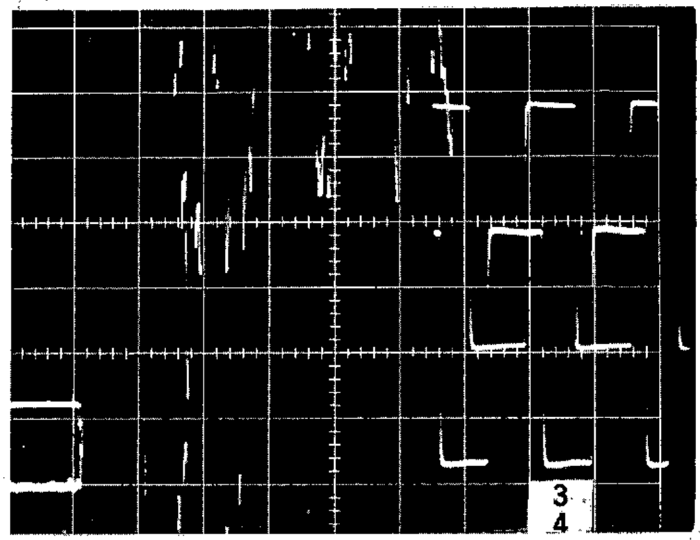

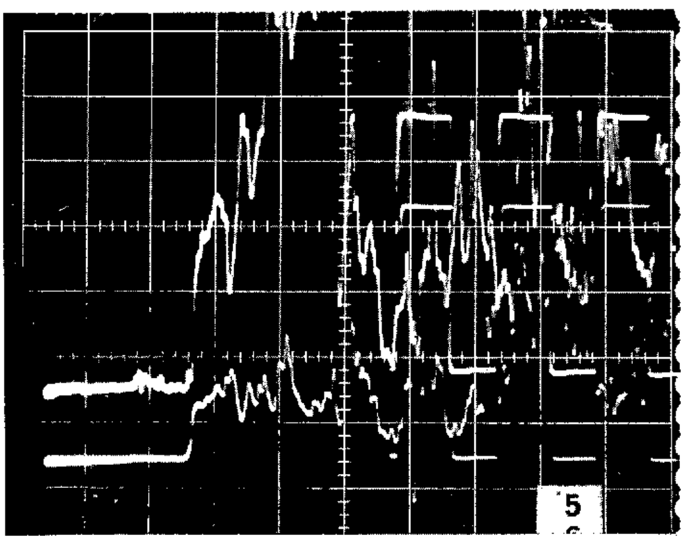

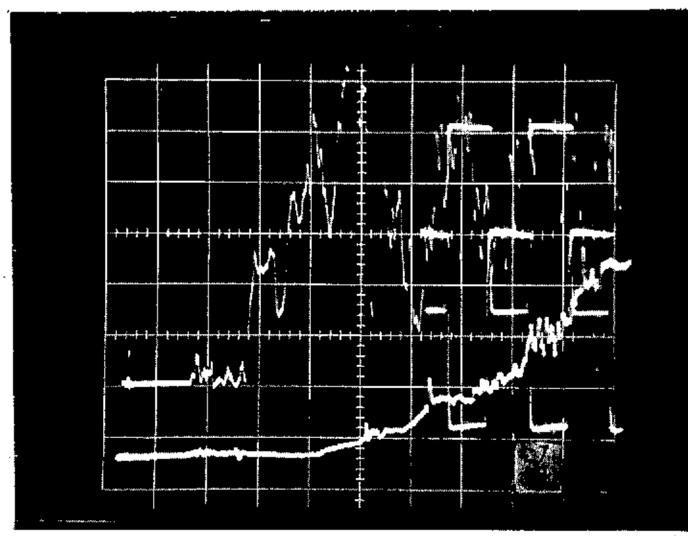

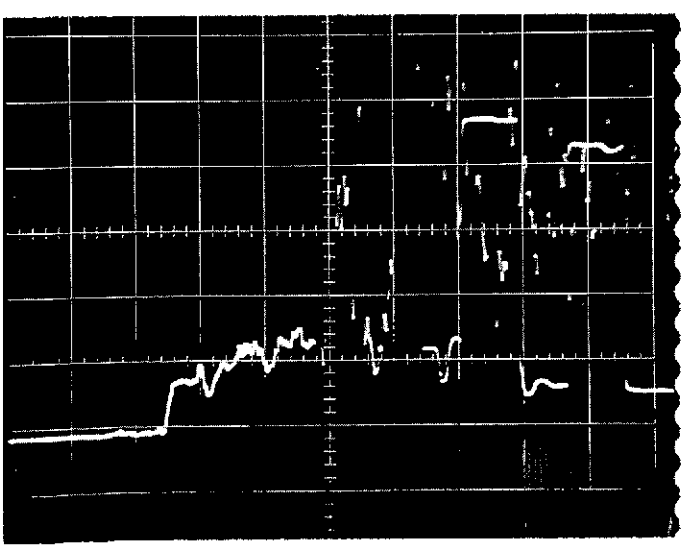

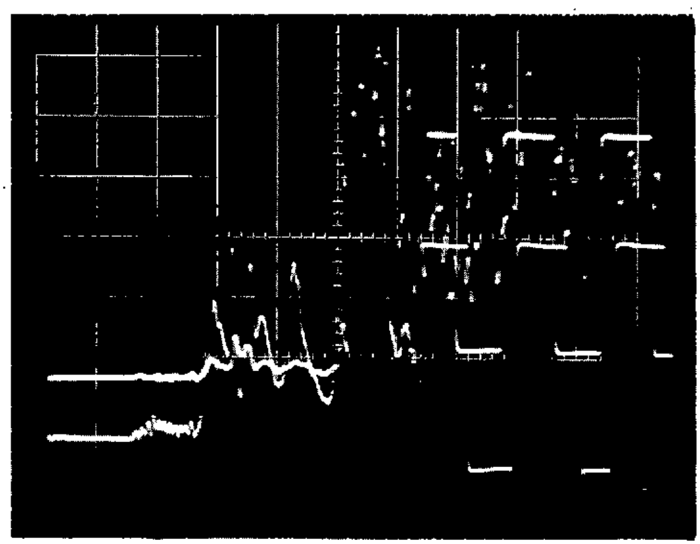

CALSPAN CORPORATION

Aerodynamic Research Department

2

Program 15"0"

W. A. ______ Date 12-10-73 Run 113

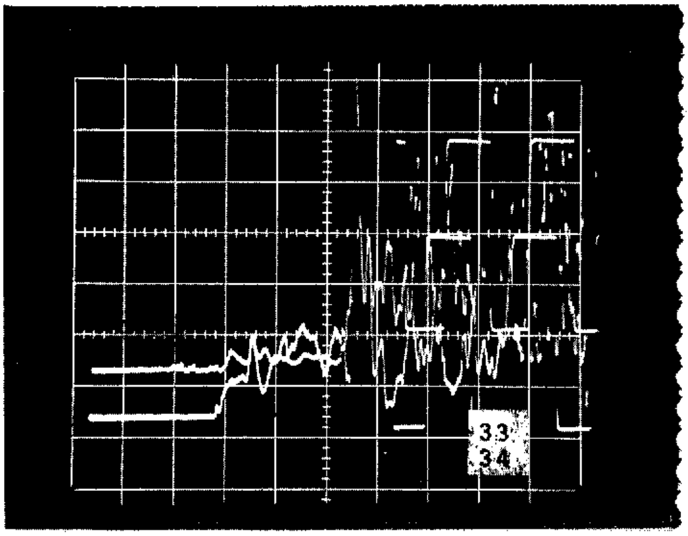

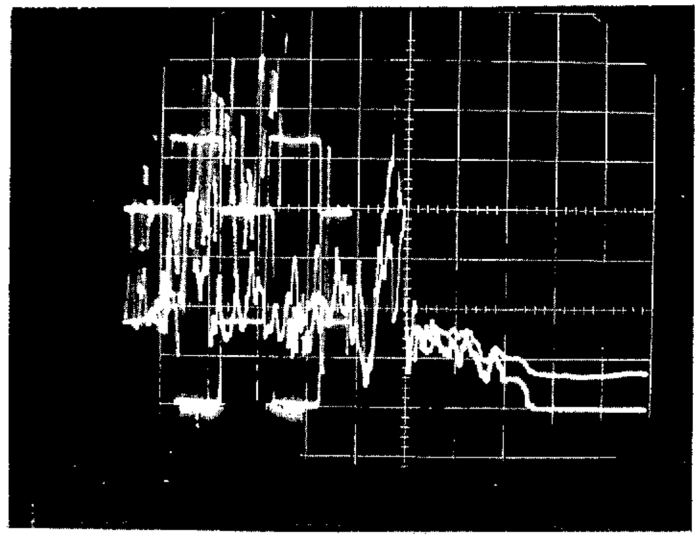

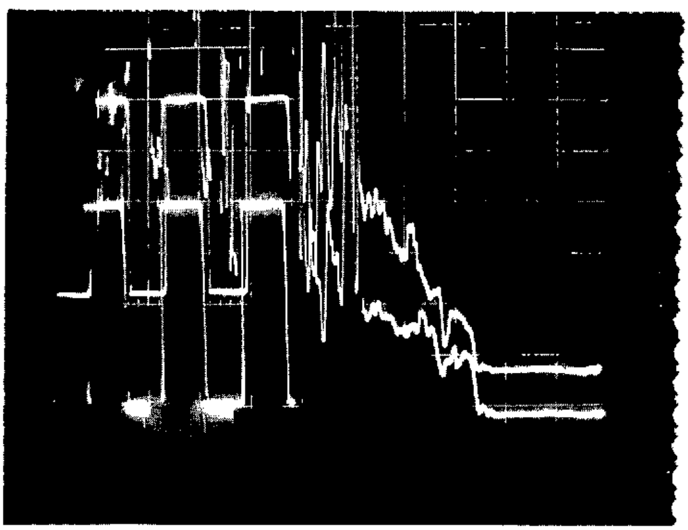

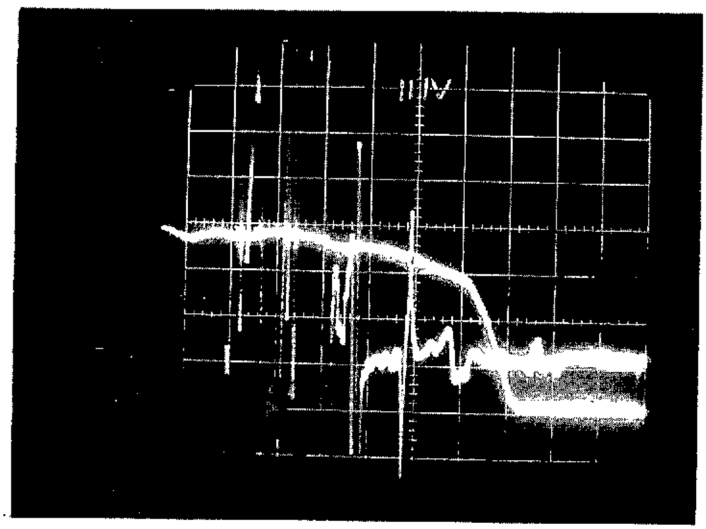

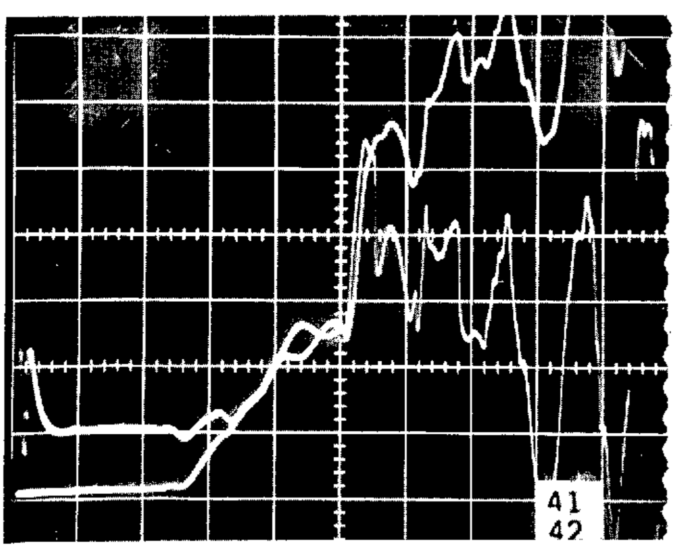

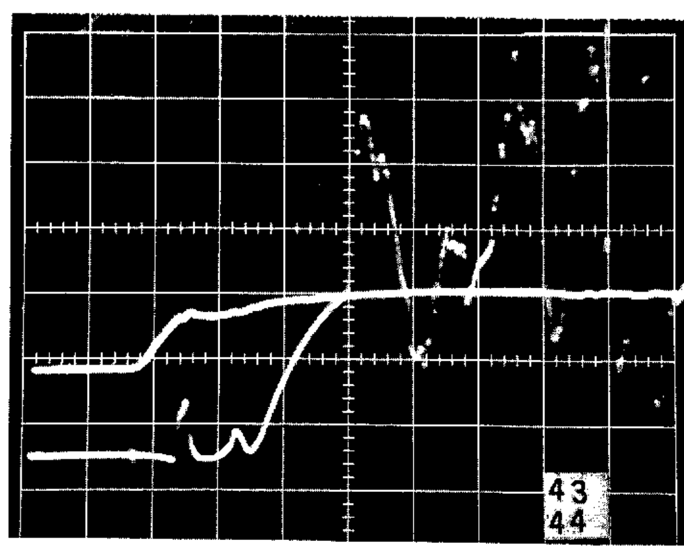

CALSPAN CORPORATION

Aerodynamic Research Department

(3)

Program 25 "0"

W. A. ______ Date 12-10-73 Run 113

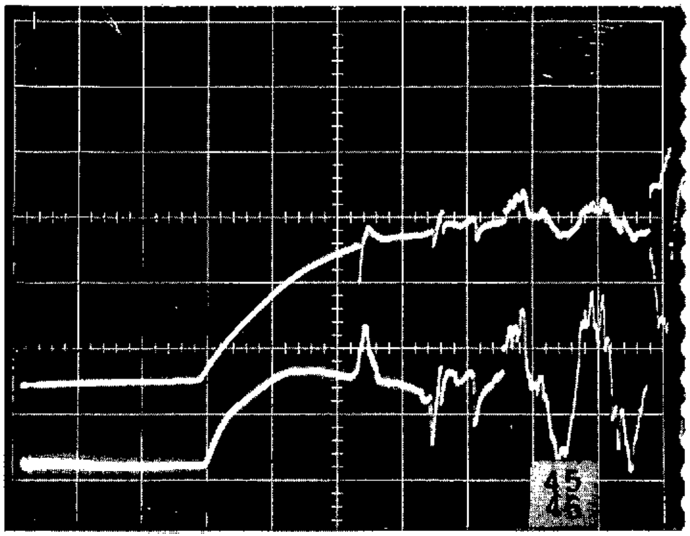

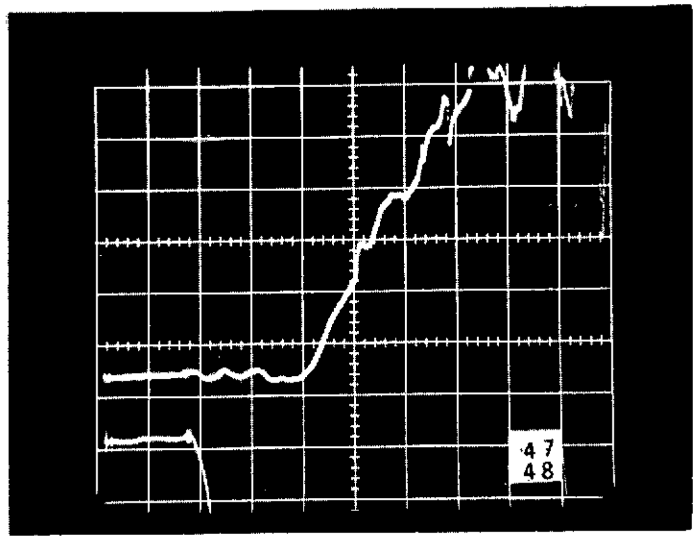

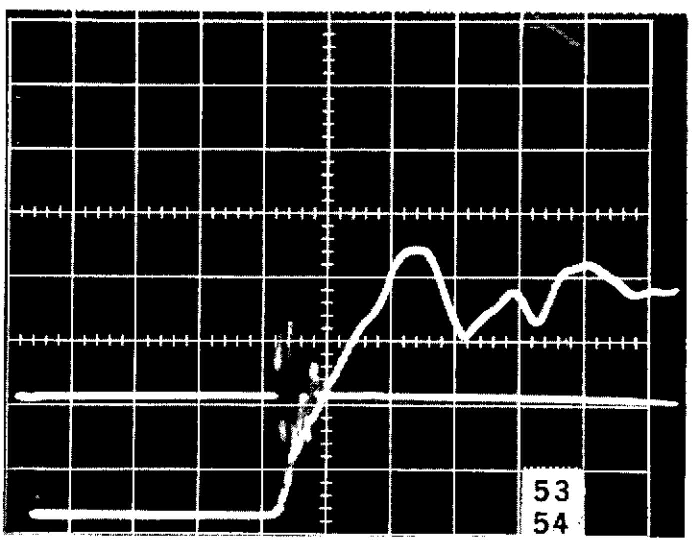

$\overline{P_c}_{(SSME)}$ = 1060 PSIA; $\overline{P_c}_{(OMS)}$ = 100 PSIA
ALT = 230,000 FT (38μ)

RUN 114

SCOPE CHANNEL	SENSOR	K (Ω/$^\circ$F)	PRE-RUN R (Ω)	DLR (K-Ω)	SWEEP (MSEC/CM)					
1	Q46	0.134	106	100	5					
2	Q53	0.125	101	150						
3	Q54	0.139	OPEN	—						
4	Q59	0.115	95	10						
5	Q64	0.121	98	10						
6	Q66	0.135	107	20						
7	Q70	0.115	100	40						
8	QR32	0.142	103	400						
9	Q98	0.099	85	100						
10										
31	Q87	0.133	106	200						
32	Q89	0.139	113	200						
33	Q91	0.121	106	200						
34	Q92	0.096	83	200						
35	Q95	0.102	93	100						
36	Q97	0.096	89	200						
37	Q101	0.158	127	80						
38	Q107	0.140	110	100						
39	Q109	0.127	OPEN	—						
40	P_c (OMS 1)	22.7*		1000 MV/CM						
41	P30	1741*		10						
42	P32	1603*		20						
43	P_c (SSME 1)	1.925*		1000						
44	PNE (SW #1)	154*		100						
45	PNE (SW #2)	215*		200						
46	PNE (SW #3)	225*		200						
47	PNE (OMS 1)	371*		50						

* MV/PSI.

CALSPAN CORPORATION

Aerodynamic Research Department

1

Program 25 "0"

W. A. ______ Date 12-12-73 Run 114

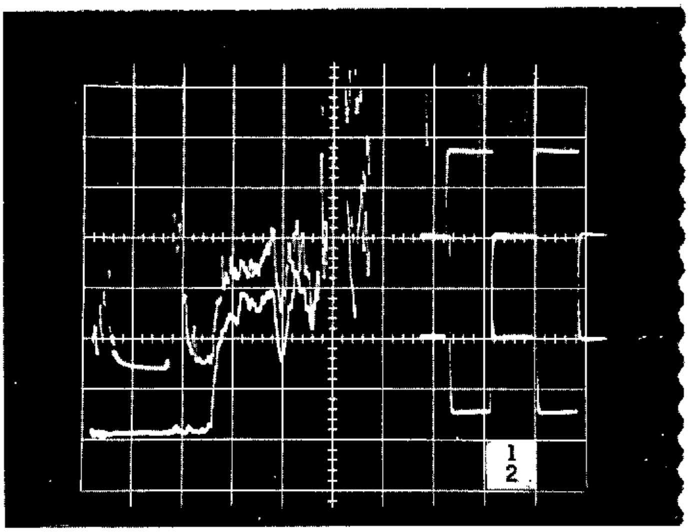

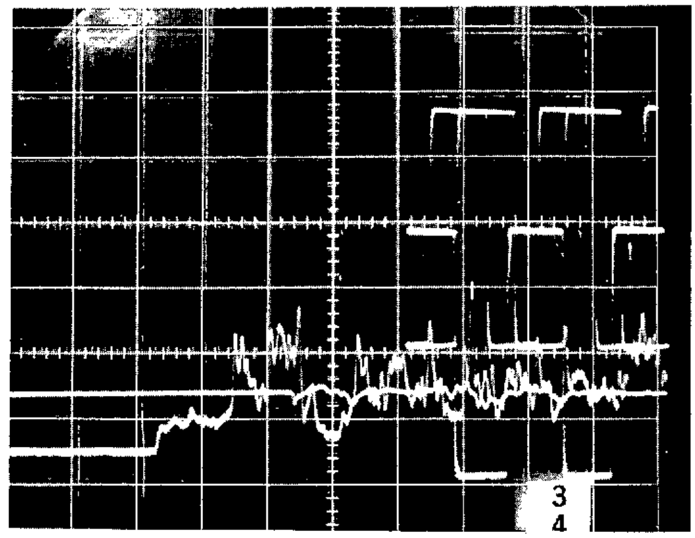

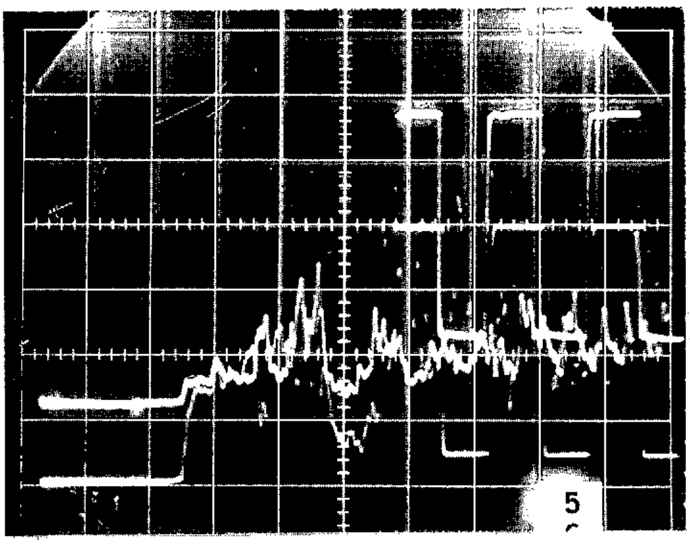

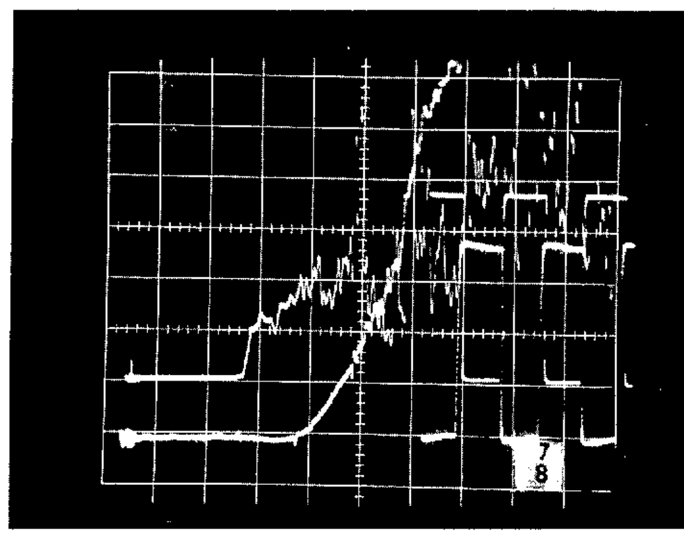

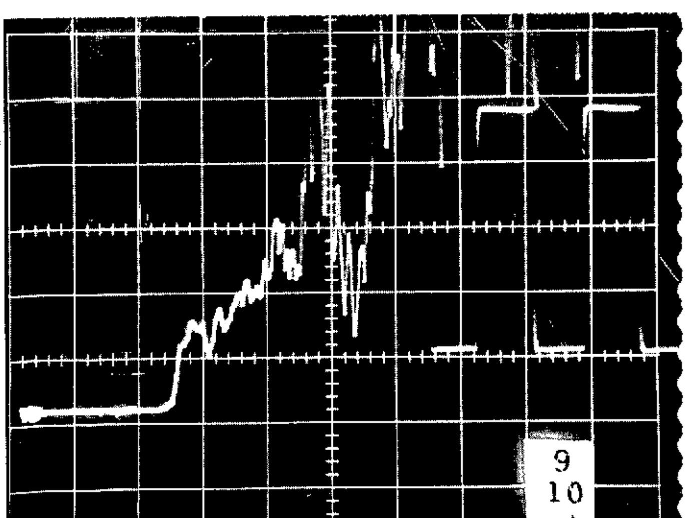

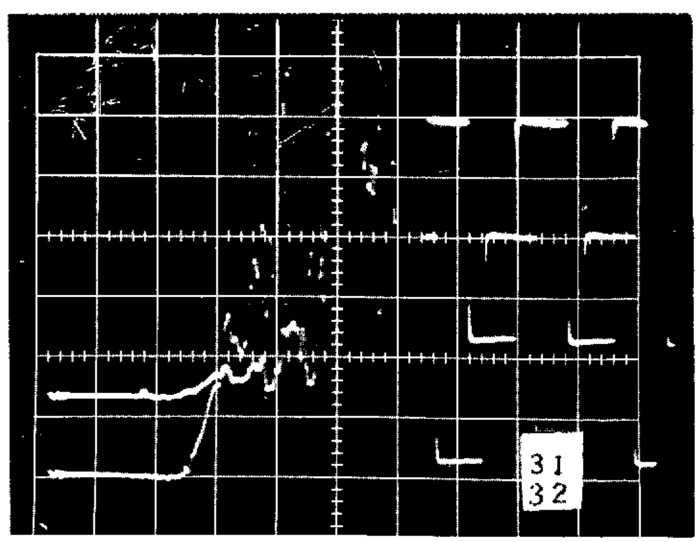

(2)

CALSPAN CORPORATION

Aerodynamic Research Department

Program 25"Ø

W. A. ______ **Date** 12-12-73 **Run** 114

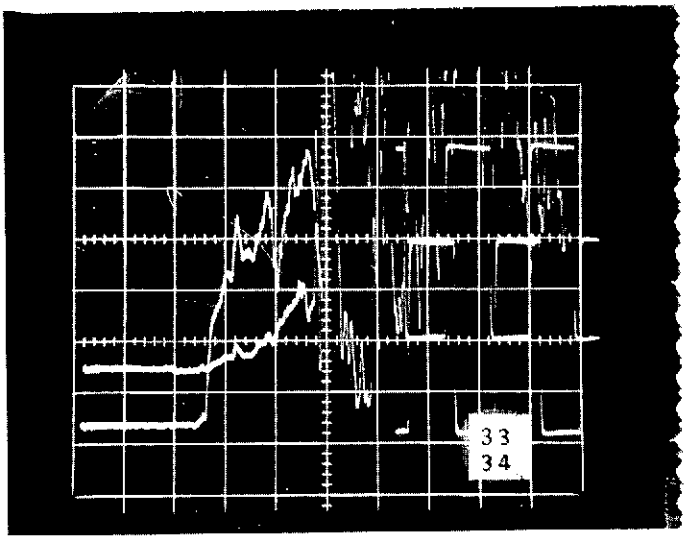

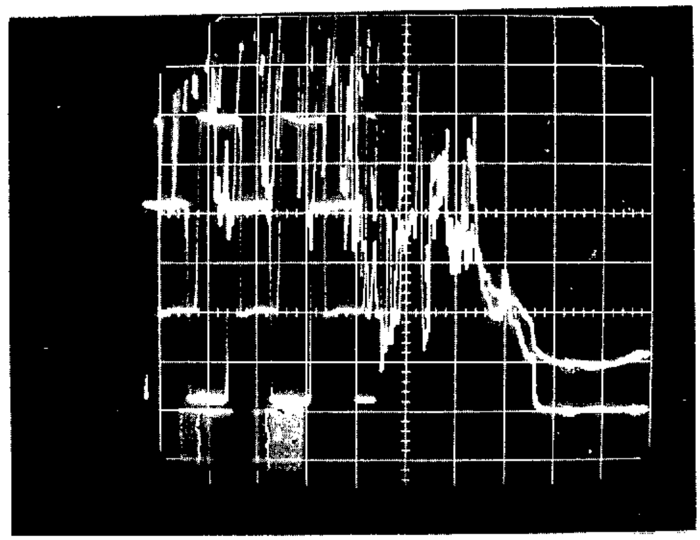

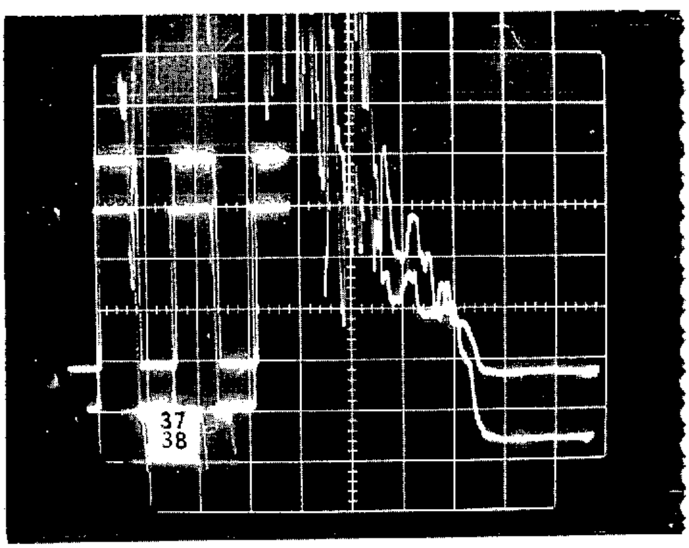

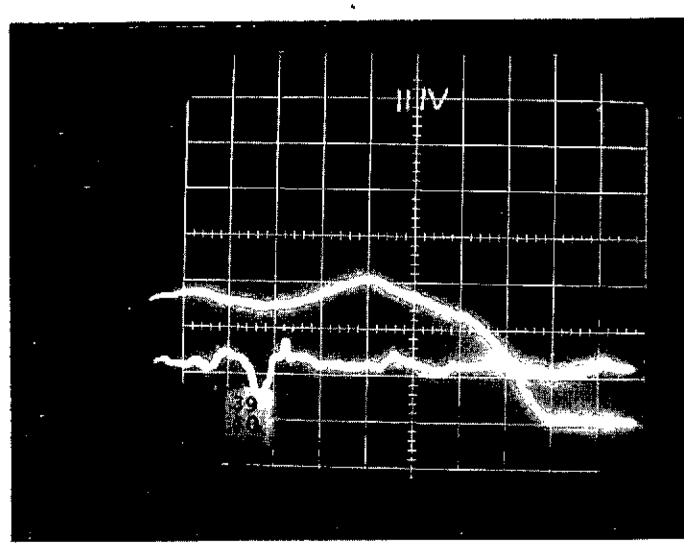

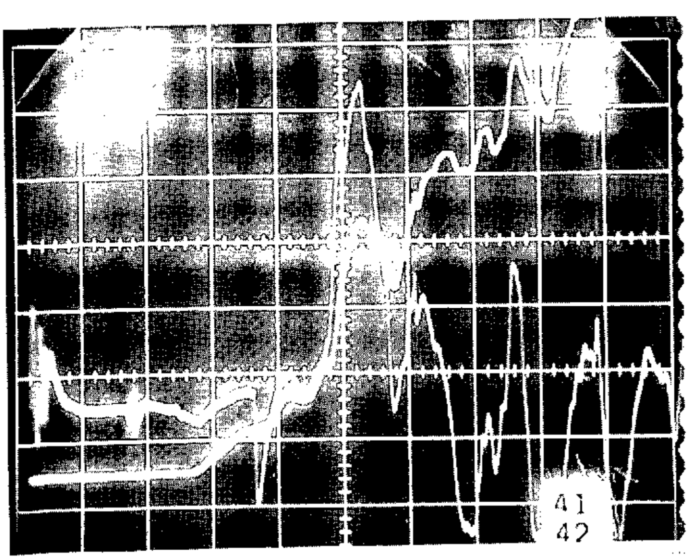

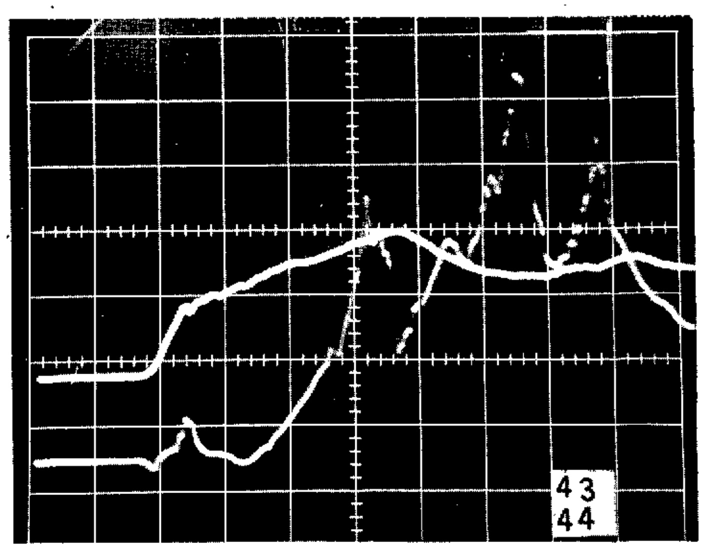

CALSPAN CORPORATION

Aerodynamic Research Department

(3)

Program 25 "0

W. A. ________ Date 12-12-73 Run 114

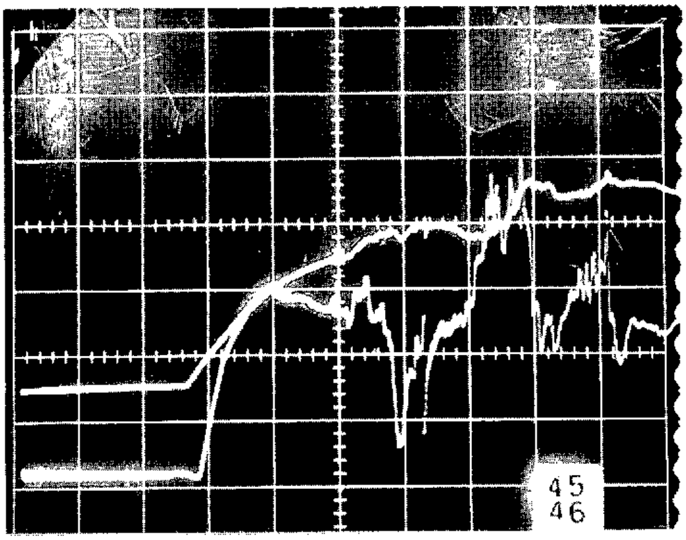

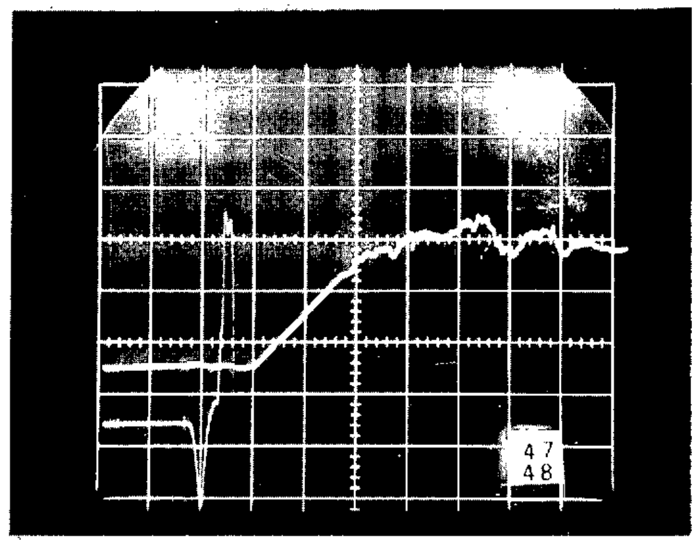

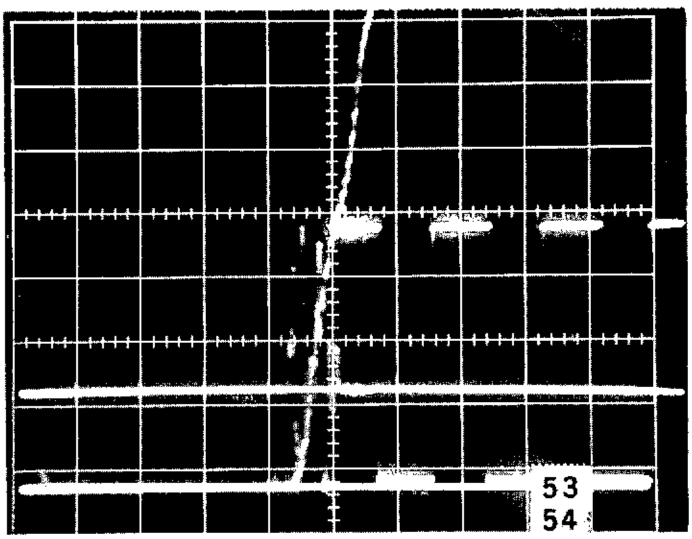

ORIGINAL PAGE IS
OF POOR QUALITY

$\overline{P}_{c(SSME)}$ = 1060 PSIA, $\overline{P}_{c(OMS)}$ = 98 PSIA.
ALT = 210,000 FT (100μ)

RUN 115

SCOPE CHANNEL	SENSOR	K (Ω/°F)	PRE-RUN R (Ω)	DLR (K-Ω)	SWEEP (MSEC/CM)
1	Q46	0.134	103	100	5
2	Q53	0.125	100	150	
3	Q54	0.139	OPEN	—	
4	Q59	0.115	92	10	
5	Q64	0.121	97	10	
6	Q66	0.135	107	20	
7	Q70	0.113	97	40	
8	Q292	0.142	101	400	
9	Q78	0.099	84	100	
10					
31	Q87	0.133	105	200	
32	Q89	0.134	112	200	
33	Q91	0.121	102	200	
34	Q92	0.096	83	200	
35	Q95	0.102	91	100	
36	Q97	0.096	87	200	
37	Q101	0.158	122	80	
38	Q107	0.140	109	100	
39	Q109	0.127	OPEN	—	
40	Pc (OMS 1)	22.7*		1000 MV/CM	
41	P30	1741*		10	
42	P32	1603*		20	
43	Pc (SSME 1)	1.925*		1000	
44	PNE (SSME #1)	154*		100	
45	PNE (SSME #2)	215*		200	
46	PNE (SSME #3)	225*		200	
47	PNE (OMS 1)	371*		50	

* MV/PSI.

CALSPAN CORPORATION

Aerodynamic Research Department

Program 25-0

W. A. I69-220 Date 12 DEC 73 Run 115

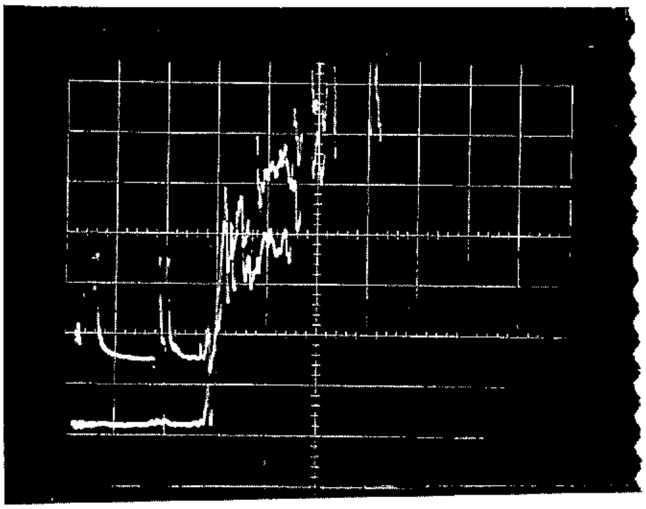

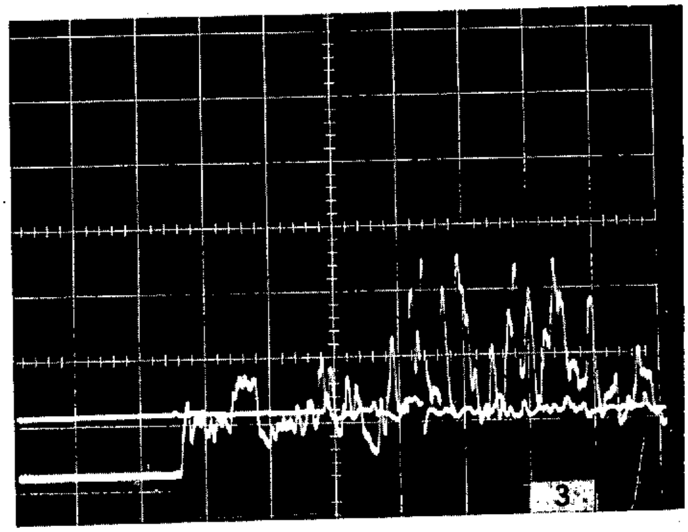

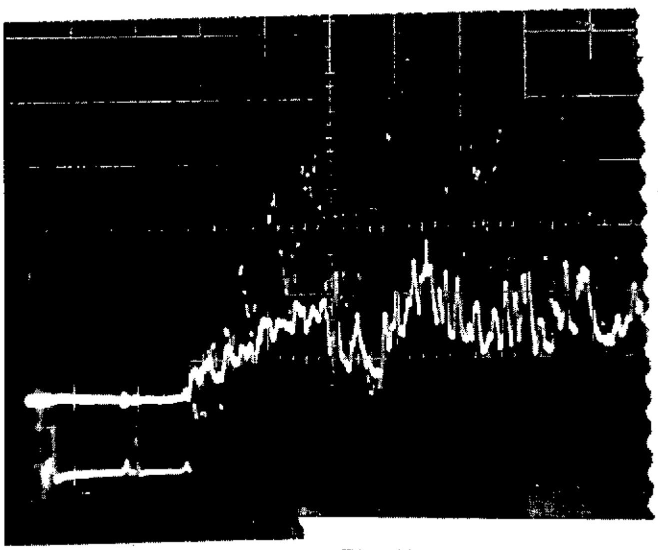

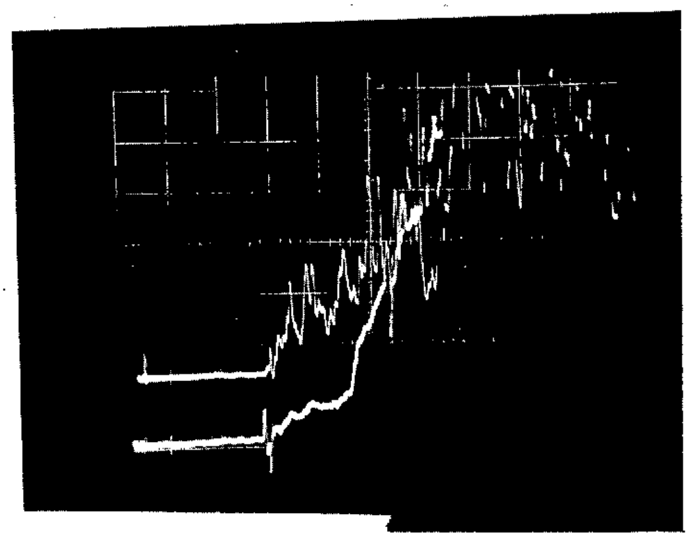

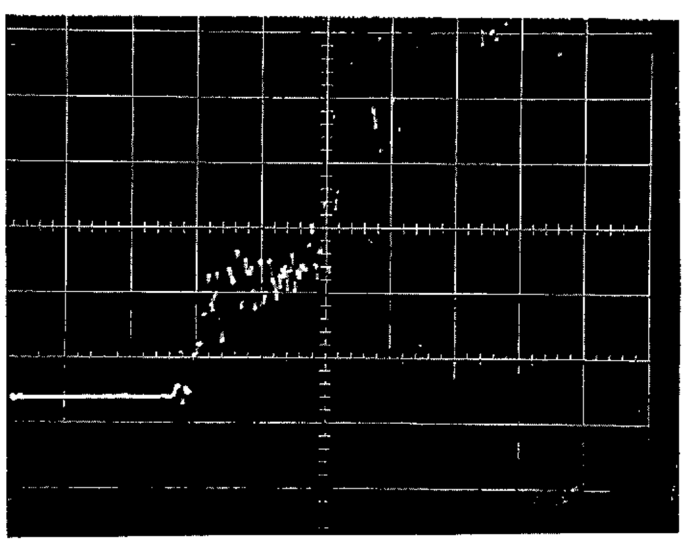

(2)

CALSPAN CORPORATION

Aerodynamic Research Department

Program 25-0

W. A. I69-220 Date 12 DEC 73 Run 115

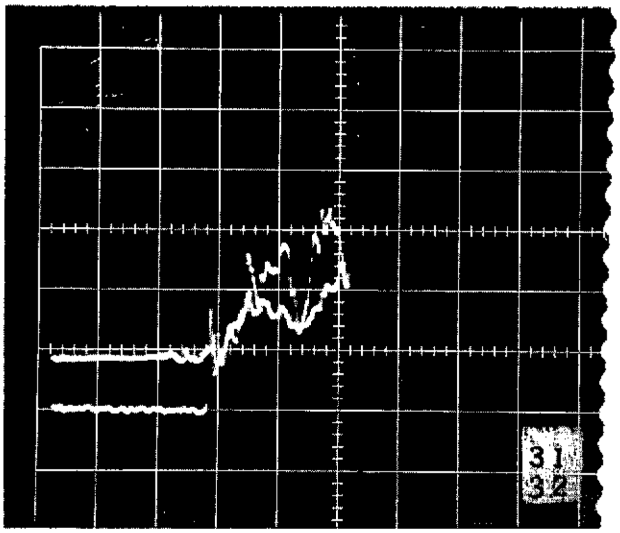

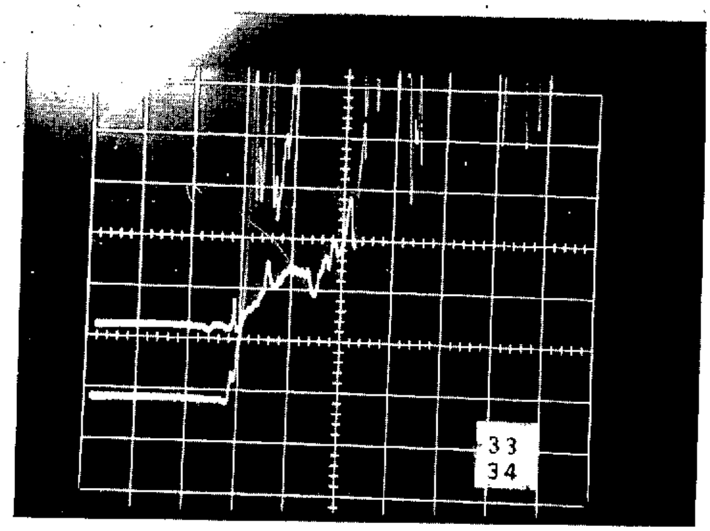

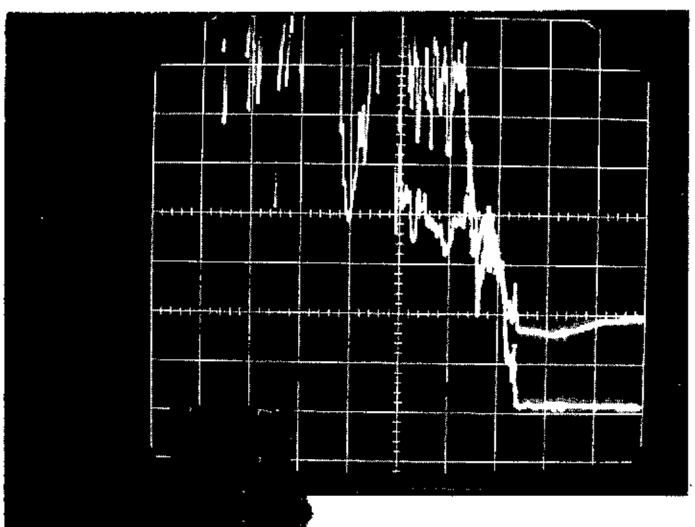

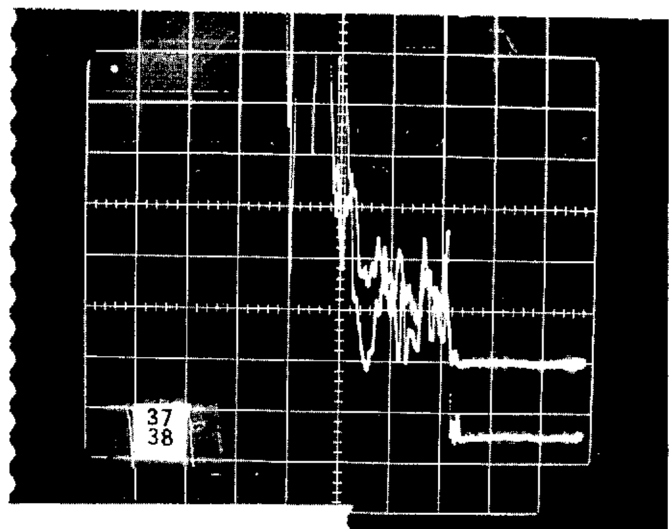

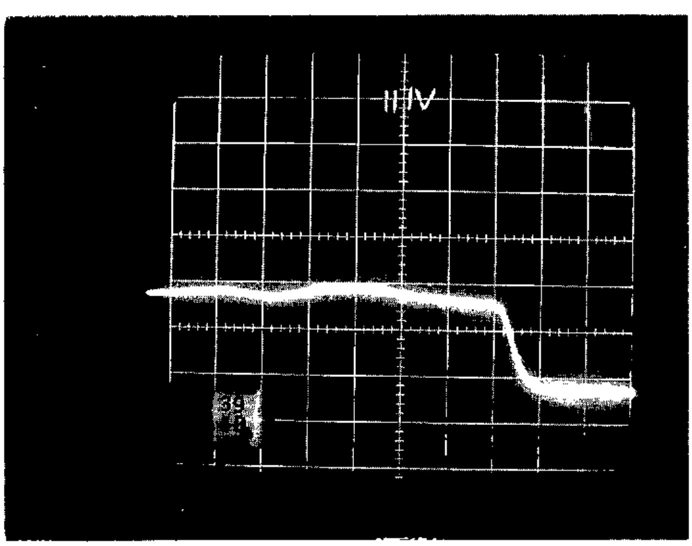

(3)

CALSPAN CORPORATION

Aerodynamic Research Department

Program 25-0

W. A. I69-220 Date 12 DEC 73 Run 115

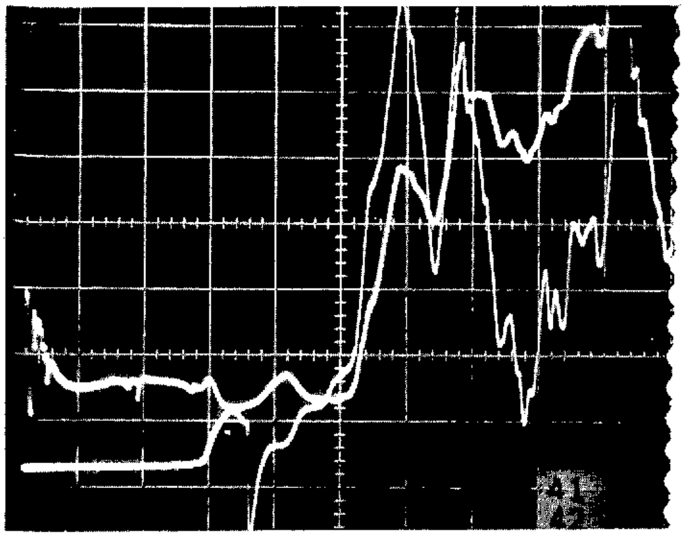

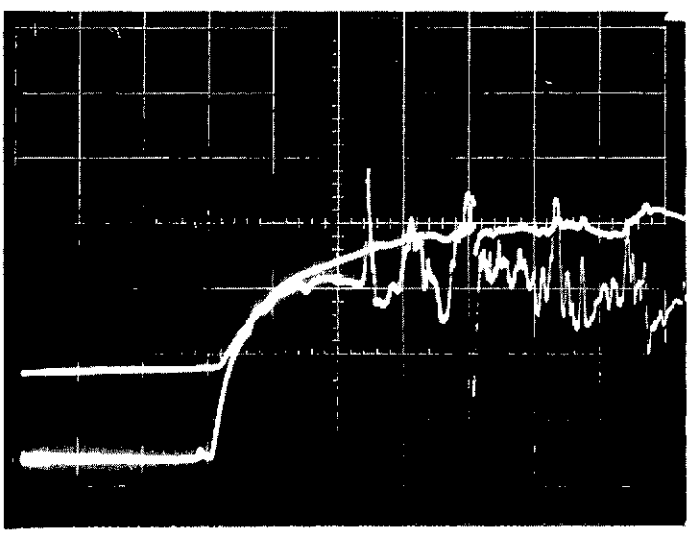

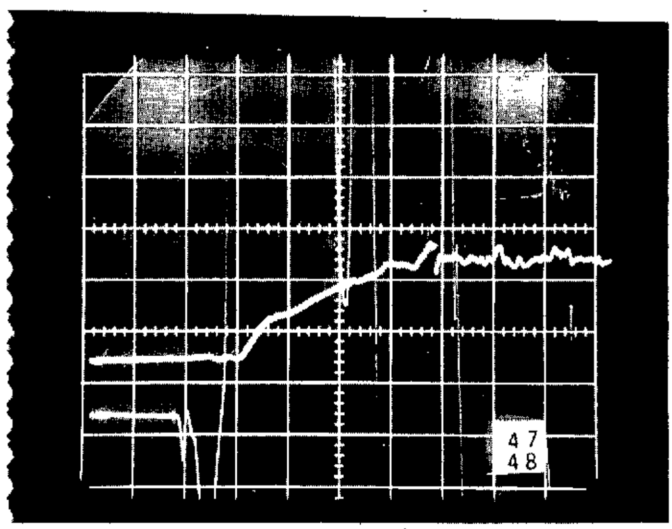

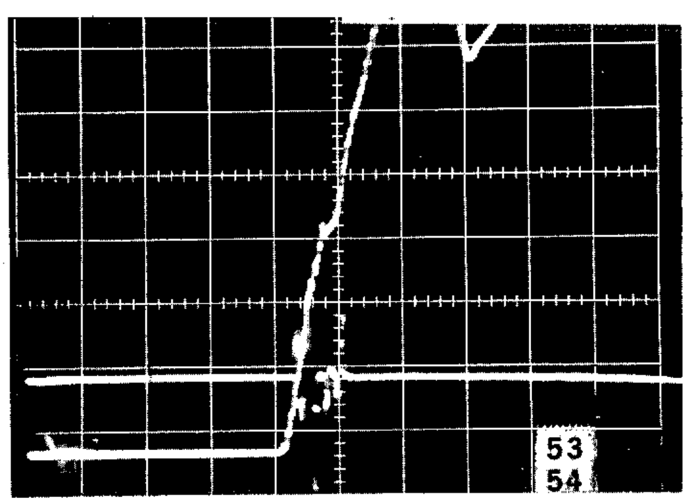

SECTION II N75 20450

CORRELATION PARAMETERS FOR THE STUDY OF LEESIDE HEATING ON A LIFTING BODY AT HYPERSONIC SPEEDS

R. J. Vidal

Introduction

An important problem in the space shuttle technology program is one of heat transfer to the leeside of shuttle orbiter configurations during high angle of attack reentry. The flow on the leeside presumably is separated, and the heat transfer to that surface should be a small fraction of the heat transfer to the windward surface. In anticipation of this possibility, the preliminary orbiter designs have relied on conventional lightweight structures for the large leeside surfaces, thereby effecting important savings in weight. However, basic questions remain concerning (1) the magnitude of the leeside heating rates and (2) the methods to be used to extrapolate wind tunnel leeside heating rates to the full-scale flight condition.

A short study of leeside heating has been made at Calspan with the aim of gaining some insight into the two problems cited above. This study was based on using existing experimental data obtained in the Calspan hypersonic shock tunnels on lifting body configurations that are typical of shuttle orbiter vehicles. The study was restricted to a configuration developed by the Convair Aerospace Division of the General Dynamics Corporation, and identified as the Multipurpose Reuseable Spacecraft (MRS). The configuration and other data from this configuration have been reported in the literature.[1] The data from the Calspan experiments have been published in a report to the contractor,[2] and the data given here were taken from Ref. 2.* These data were obtained at Mach numbers of 8 and 10, at angles of attack from 0° to 30°, and over a unit Reynolds number range of 1.7×10^6 to 80×10^6 per foot.

The planned method of approach was first to examine the heat transfer to the windward surface of the body in order to determine if the windward boundary layer was laminar, transitional, or turbulent. With this information in hand, the data could be classified as laminar or turbulent, and finally the leeside heating within that classification could be examined. It was not

* The author would like to express his thanks to Mr. Gail Schadt at the General Dynamics Corporation for his permission to use and to publish those data.

necessary to pursue this plan to completion, however, because a reasonably good correlation of all data was obtained within the parameters for laminar boundary layers.

The details of the correlation study are given in the following paragraphs in the chronological order in which they were pursued, i.e., the correlations for the windward turbulent boundary layer, the correlations for the windward laminar boundary layer, and the correlations for the leeside surfaces. There are two key conclusions reached from this study. First, a consistent correlation does not appear to be feasible within the framework of existing turbulent boundary layer theories, either for attached or separated flows, evidently because the theories are restricted to constant pressure flow fields. Second, consistent correlations appear to be feasible within the framework of laminar boundary layer similarity parameters when both the local pressure and the pressure distribution are taken into account.

Turbulent Boundary Layer

The data correlations for the windward turbulent boundary layer were made within the framework of the Spaulding and Chi theory.[3] Briefly stated, that theory applies only for flat plate flows with no pressure gradient, and it is based upon extensive empirical correlations of experimental data obtained from many sources. The end result is that a broad range of experimental skin friction data can be correlated in terms of the Reynolds number and two parameters, F_c and F_{R_δ}, which are functions of only the Mach number at the edge of the boundary layer and the ratio of the wall temperature to the gas temperature at the edge of the boundary layer. The Reynolds number is based on conditions at the edge of the boundary layer. The correlation is obtained in terms of $F_c\ C_f$ and $\frac{F_{R_\delta}}{F_c} Re_x$, where C_f is the local skin friction coefficient and Re_x is the Reynolds number based on the distance, x, from the leading edge.

Application of the Spaulding-Chi theory requires that the local inviscid conditions be determined. In the first correlations attempted, theoretical methods were used to calculate the local inviscid conditions. In particular, the available pressure data were compared with Cheng's theory for blunted cones[4] and it was found that the data correlated reasonably well if the local inclination of the surface was taken as the cone half angle, θ. Cheng's theory was then approximated by the following formula which is a linear superposition of the effect of cone angle and the effect of nose bluntness,

$$\frac{1}{\gamma M_\infty^2 \theta^2} \cdot \frac{p}{p_\infty} \approx 1 + \frac{0.18}{\frac{\theta^2}{\sqrt{\epsilon k}} \frac{x}{d_n}} \tag{1}$$

where θ is the cone half angle, $\epsilon = \frac{\gamma - 1}{\gamma + 1}$, k and d_n are the nose drag coefficient and the nose diameter, and x is the streamwise coordinate. This relation was used to predict the local pressure in the flowfield. The density ratio and temperature ratio across the conical shock wave were estimated by assuming that these ratios could be represented by similar ratios consistent with the shock wave on a blunted wedge. The assumption for density ratio is reasonable and is verified for sharp cones, by the tabulated date in Ref. 5. The technique used was to cast the wedge relations for density and temperature into a form such that pressure was the independent variable.

$$\frac{\rho_\infty}{\rho_G} = \epsilon + \frac{4\gamma}{(\gamma+1)^2} \left(\frac{p_G}{p_\infty} + \epsilon \right) \tag{2}$$

$$\frac{T_G}{T_\infty} = \epsilon \frac{p_G}{p_\infty} + \frac{4\gamma}{(\gamma+1)^2} \left[1 - \frac{\epsilon}{\epsilon + \frac{p_G}{p_\infty}} \right] \tag{3}$$

where the subscripts, ∞ and G, refer to ambient and local conditions.

A correlation was attempted using these approximations, and it was found that the scatter was excessive. The source of the scatter was judged to be the approximate method used to calculate pressure, and consequently the next method used was based on the experimental pressure data. Typical data obtained in the windward plane of symmetry are shown in Fig. 1. These were faired as indicated, and those faired data were used in conjunction with Eq. 2 and 3 to calculate the local inviscid flow properties.

The correlation generated within the Spaulding-Chi parameters is shown in Fig. 2, with some data for the leeward surface shown by the flagged symbols. After considerable analysis, it was concluded that all data for $\frac{F_{R_\delta}}{F_c} Re_x \leq 3\times10^6$ and all leeside data shown in Fig. 2 should be ignored in this correlation because they correspond to laminar conditions and hence, a correlation can not be expected within the parameters for turbulent boundary layers. The remaining data, those lying above the Spaulding-Chi theory, show a tenuous correlation which is, for practical purposes, insensitive to Reynolds number. It is believed that the poor correlation in those data stems from the fact that the Spaulding-Chi parameters do not apply to these data because the flow field is not a constant pressure flow field. The parameters were calculated at each local condition and no allowance could be made for the pressure history of the boundary layer. It is well documented in the literature that turbulent boundary layers are very sensitive to pressure history, the so-called non-equilibrium turbulent boundary layers, and no generalized comparisons have been obtained between them and constant-pressure turbulent boundary layers.

Laminar Boundary Layer

The contention that the data in Fig. 2 falling below $\frac{F_{R_\delta}}{F_c} Re_x \lesssim 3\times10^6$ are in a laminar or transitional range is verified in Fig. 3 where those data are compared with Cheng's theory[4] for the laminar boundary layer on a blunted cone. The oscillations in the theoretical solution should be ignored[4] because Cheng notes that they probably arise from instabilities in the numerical solution. The data do show that for these three runs, the boundary layer on the windward plane of symmetry was at least partially laminar. Since these data were obtained for $\frac{\theta^2}{\sqrt{\epsilon k}} \frac{x}{d_n} \approx O(1)$ the indications are that nose-bluntness effects are negligible, and a valid comparison can be made by specializing Cheng's parameters for this case. This specialization yields the following

$$C_H = 0.332 \sqrt{\frac{C_*}{Re_d}} \sqrt{\frac{d_n}{x}} \sqrt{\frac{p}{p_\infty}} \tag{4}$$

where the constant, 0.332, is the solution at the surface for the Blasius equation. The parameter, C_*, is Cheng's modification of the Chapman-Rubesin constant, and is defined as

$$C_* = \frac{T_\infty}{T_*} \frac{\mu(T_*)}{\mu(T_\infty)} \qquad T_* = \frac{T_o}{6}\left[1 + 3\,\frac{T_w}{T_o}\right] \tag{5}$$

where T_o is the stagnation (enthalpy) temperature.

The parameters in Eq. 4 were evaluated using the experimental pressure distributions, and the resulting correlation are shown in Fig. 4. These show that the laminar heating rates on this configuration are somewhat less than the Blasius solution, but the data for Run 14 clearly are laminar because they exhibit a $\sqrt{x}$-dependence. The fact that the initial data for the other two runs agree well with Run 14 demonstrate that those initial data are laminar and that the downstream data are transitional.

Generalized Laminar Similarity Parameters

This application of Cheng's similarity parameters has indicated that improved correlations for the leeside heating might be obtained by reverting to the most general form for the similarity parameters. Briefly, Cheng's analysis centers on a transformation of the laminar boundary layer equations using a modified form of the Howarth-Dorodnitsyn-Levy-Lees parameters, namely

$$\frac{u}{U_\infty} = \mathcal{O}_\eta \qquad \Theta = \frac{H - H_w}{H_\infty - H_w}$$
$$\xi = \int_0^x C_* \frac{p}{p_\infty}\frac{dx}{L} \qquad \eta = \sqrt{\frac{Re_L}{\xi}} \int_0^y \frac{\rho}{\rho_\infty}\frac{dy}{L} \tag{6}$$

where H is the total enthalpy and L is a reference length. With this transformation and for hypersonic conditions, the boundary layer equations reduce to the Blasius equation, and it is concluded that $\mathcal{O}_\eta \equiv \Theta$. With this development, it is possible to write down directly a general expression for laminar heat transfer to a surface with an arbitrary pressure distribution.

$$M^3 C_H = 0.332\, M^3 \sqrt{\frac{C_*}{Re_x}} \; \frac{p/p_\infty}{\sqrt{\int_0^L \frac{p}{p_\infty}\frac{dx}{L}}} \tag{7}$$

The apparent redundancy in M^3 is required rigorously in order to preserve the similarity parameter, $M^3 \sqrt{\frac{C_*}{Re_x}}$. However, this form was not used in the correlation that follows because most of the data were obtained at $M \approx 8$. Accordingly, the similarity parameters were simplified to the following as the ordinate and abscissa for a correlation graph

$$\text{Ordinate} \equiv C_H \qquad \text{Abscissa} \equiv \frac{Re_x}{C_*} \frac{\int_0^L \frac{p}{p_\infty} \frac{dx}{L}}{\left(\frac{p}{p_\infty}\right)^2} \tag{7a}$$

The generalized similarity parameter, Eq. 7a, has been applied to correlate heat transfer data obtained on the leeside center line by using experimental pressure data to evaluate the integral in Eq. 7a. The pressure data are shown in Fig. 5 along with simplified fairings used to approximate the data. These fairings correspond to the linear approximation

$$\begin{aligned} \text{For} \quad & \frac{x}{d_n} < C_3 \; ; \quad \frac{p}{p_\infty} = C_1 \\ & \frac{x}{d_n} > C_3 \; ; \quad \frac{p}{p_\infty} = C_1 - C_2 \left(\frac{x}{d_n} - C_3\right) \end{aligned} \tag{8}$$

These can be evaluated to yield

$$\begin{aligned} \text{For} \quad & \frac{x}{d_n} < C_3 \; ; \quad \int_0^L \frac{p}{p_\infty} \frac{dx}{L} = C_1 \\ & \frac{x}{d_n} > C_3 \; ; \quad \int_0^L \frac{p}{p_\infty} \frac{dx}{L} = \frac{p}{p_\infty} + \frac{C_2}{2} \left(\frac{x}{d_n} - \frac{C_3^2}{x/d_n}\right) \end{aligned} \tag{9}$$

Eq. 9 was used with the experimental pressures to evaluate the governing parameters in Eq. 7a. The correlation of heating rates on the leeside center line are shown in Fig. 6. It can be seen that a reasonably good correlation is obtained with these parameters, with scatter of about ±30%. There is some contradictory behavior at low Reynolds numbers (or higher Mach number) that can not be resolved within these data because the data are sparse in that range. However, it is clear that for values of the abscissa (which essentially is the Reynolds number) greater than about 2×10^6, the leeside heating exhibits a Reynolds number dependence which approaches a 1/3 power of the abscissa. For values of the abscissa less than 2 x 10^6, the evidence is sparse but the available data suggest almost no Reynolds number dependence.

There are a number of observations that can be made in Fig. 6. First, a comparison of the correlation with the Blasius solution shows the data lie above the theory and it raises the question of whether or not the leeside flow was separated. This question was assessed by examining the data obtained at zero angle of attack. Those data, not shown in Fig. 6, are a factor of 2 to 4 times higher than the leeside data. This comparison suggests that the leeside data shown in Fig. 6 correspond to a separated flow. The data at zero angle of attack are also a factor of 4 to 10 higher than the Blasias solution. This indicates that the boundary layer was turbulent.

A curve is shown in Fig. 6 for the theoretical stagnation point heat transfer. This theoretical value corresponds closely to the Fay-Riddell theory[6] evaluated for a Lewis number of unity. It should be emphasized that a direct comparison between leeside and stagnation point heating is not possible, and in fact, such a comparison is not meaningful in a general sense. This stems from the fact that the two heating rates are governed by different parameters. The leeside heating is governed by the length dimension, x, and the pressure in the leeside flow field. In contrast, the stagnation point heating is governed by the nose diameter and the stagnation pressure. These facts make any comparison between leeside heating and stagnation heating a function of ambient Mach number, angle of attack and scale, x/d_n.

It is accepted practive to express leeside heating rates as a fraction of the stagnation heating rate. Estimates of this ratio, $C_{H_{LS}}/C_{H_{ST}}$, have been made in this study, using the correlation curve in Fig. 6, by assuming the leeside pressure to be approximately equal to the ambient static pressure. With this assumption, $\frac{p_{ST}}{p_{LS}} \approx \gamma M_\infty^2$. Values of $C_{H_{LS}}/C_{H_{ST}}$ are tabulated in Table I for typical Mach numbers and Reynolds numbers, and for various values of x/d_n. It can be seen that, in these terms, the highest leeside heating occurs at low Mach numbers, high Reynolds numbers, and in regions close to the nose. The largest value for the cases considered is about 7% of the stagnation point heat transfer, and the lowest value is about 0.2% of the stagnation point heat transfer.

Concluding Remarks

A reasonably good correlation of leeside heating has been obtained for data obtained in the Calspan hypersonic shock tunnel over a wide range of Reynolds numbers for a lifting body configuration that is representative of a shuttle orbiter configuration. It is doubtful that this correlation can be applied directly to other orbiter configurations, but the correlation does provide a useful framework for evaluating leeside heating from orbiter wind tunnel tests. Of equal importance, it provides a basis for extrapolating wind tunnel results to flight conditions.

There are aspects of this preliminary correlation which should receive further study. First, an attempt should be made to reduce the scatter in the correlation. The scatter could stem from a number of sources. For example, in the interests of expediency, the viscous similitude parameters were not preserved, and some of the scatter could stem from that omission. The similarity parameters are valid for hypersonic conditions, and the test condition, $M \approx 8$, does not satisfy that restriction very well. Finally scatter could result from the linear representation of the leeside pressure distribution.

A more basic question that should be pursued is the generality of this type of correlation. It was obtained within the framework of laminar boundary layer similarity parameters, and one cannot characterize the leeside flow field as a laminar motion. A similarity analysis for turbulent flows should be made to determine the manner in which the laminar-type parameters should be modified in order to characterize the turbulent motions.

<u>References</u>

1. Young, C.H., Reda, D.C., and Roburge, A.M.: "Hypersonic Transitional and Turbulent Flow Studies on a Lifting Entry Vehicle." Paper presented at the 9th Aerospace Science Meeting, New York, Jan. 25-27, 1971, AIAA Paper No. 71-100.

2. Ryder, M.O.: "Hypersonic Aerodynamic Heating and Pressure Tests of a Lifting Body Entry Configuration." Calspan Report No. AA-2644-Y-1, December 1968.

3. Spaulding, D.B. and Chi, S.W.: "The Drag of a Compressible Turbulent Boundary Layer on a Smooth Flat Plate with and without Heat Transfer." Jour. Fluid Mech., Vol. 18, Pt. 1, Jan. 1964, pp. 117-143.

4. Cheng, H.K.: "Hypersonic Flow with Combined Leading-Edge Bluntness and Boundary Layer Displacement Effect." Calspan Report No. AF-1285-A-4, Aug. 1960.

5. Bertram, M.A.: "Correlation Graphs for Supersonic Flow Around Right Circular Cones at Zero Yaw in Air as a Perfect Gas." NASA TND-2339, June 1964.

6. Fay, J.A., and Riddell, F.R.: "Theory of Stagnation Point Heat Transfer in Dissociated Air." J.A.S., Vol. 25, No. 2, Feb. 1958, pp. 73-85.

Table I

TABULATED VALUES OF $C_{H_{LS}}/C_{H_{ST}}$ FROM FIG. 6

$\dfrac{Re_x}{C_x} \dfrac{\int_0^L p_6/p_\infty \frac{dx}{L}}{(p_6/p_\infty)^2}$	M_∞	$\frac{x}{dn} = 2$	4	10	20	40	100
10^6	10	0.0254	0.0180	0.0114	0.0081	0.0057	0.0036
	15	0.0170	0.0120	0.0076	0.0054	0.0038	0.0024
	20	0.0127	0.0090	0.0057	0.0040	0.0029	0.0018
10^7	10	0.0628	0.0444	0.0280	0.0199	0.0140	0.0089
	15	0.0425	0.0296	0.0187	0.0132	0.0093	0.0059
	20	0.0314	0.0222	0.0140	0.0100	0.0070	0.0045
10^8	10	0.0734	0.0519	0.0328	0.0232	0.0164	0.0104
	15	0.0496	0.0352	0.0218	0.0155	0.0109	0.0069
	20	0.0367	0.0260	0.0164	0.0116	0.0082	0.0052

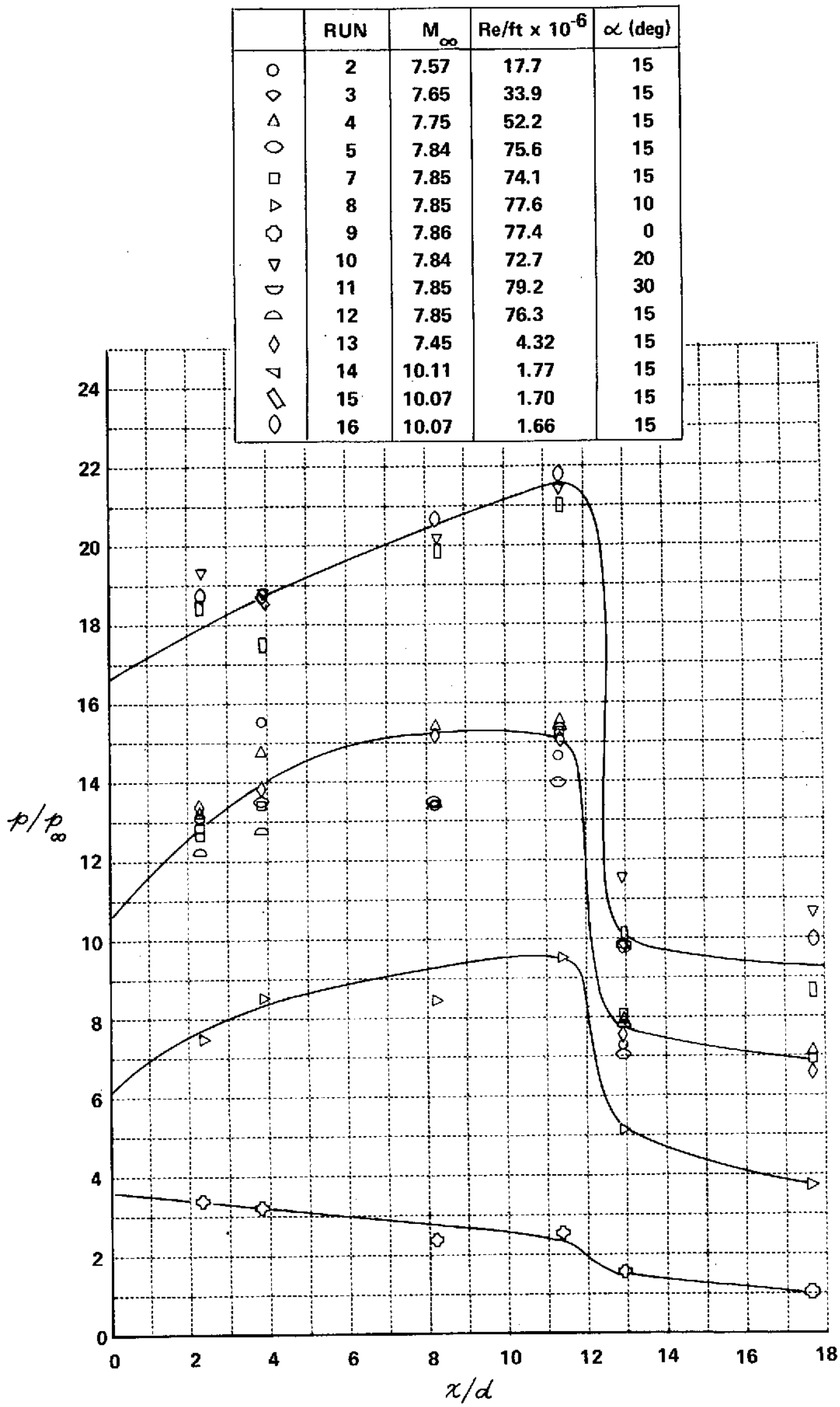

	RUN	M_∞	Re/ft x 10^{-6}	α (deg)
○	2	7.57	17.7	15
▽	3	7.65	33.9	15
△	4	7.75	52.2	15
⬭	5	7.84	75.6	15
□	7	7.85	74.1	15
▷	8	7.85	77.6	10
⬡	9	7.86	77.4	0
▽	10	7.84	72.7	20
◡	11	7.85	79.2	30
◠	12	7.85	76.3	15
◊	13	7.45	4.32	15
◁	14	10.11	1.77	15
◊	15	10.07	1.70	15
⬯	16	10.07	1.66	15

Figure 1 PRESSURE DISTRIBUTION IN THE WINDWARD PLANE OF SYMMETRY

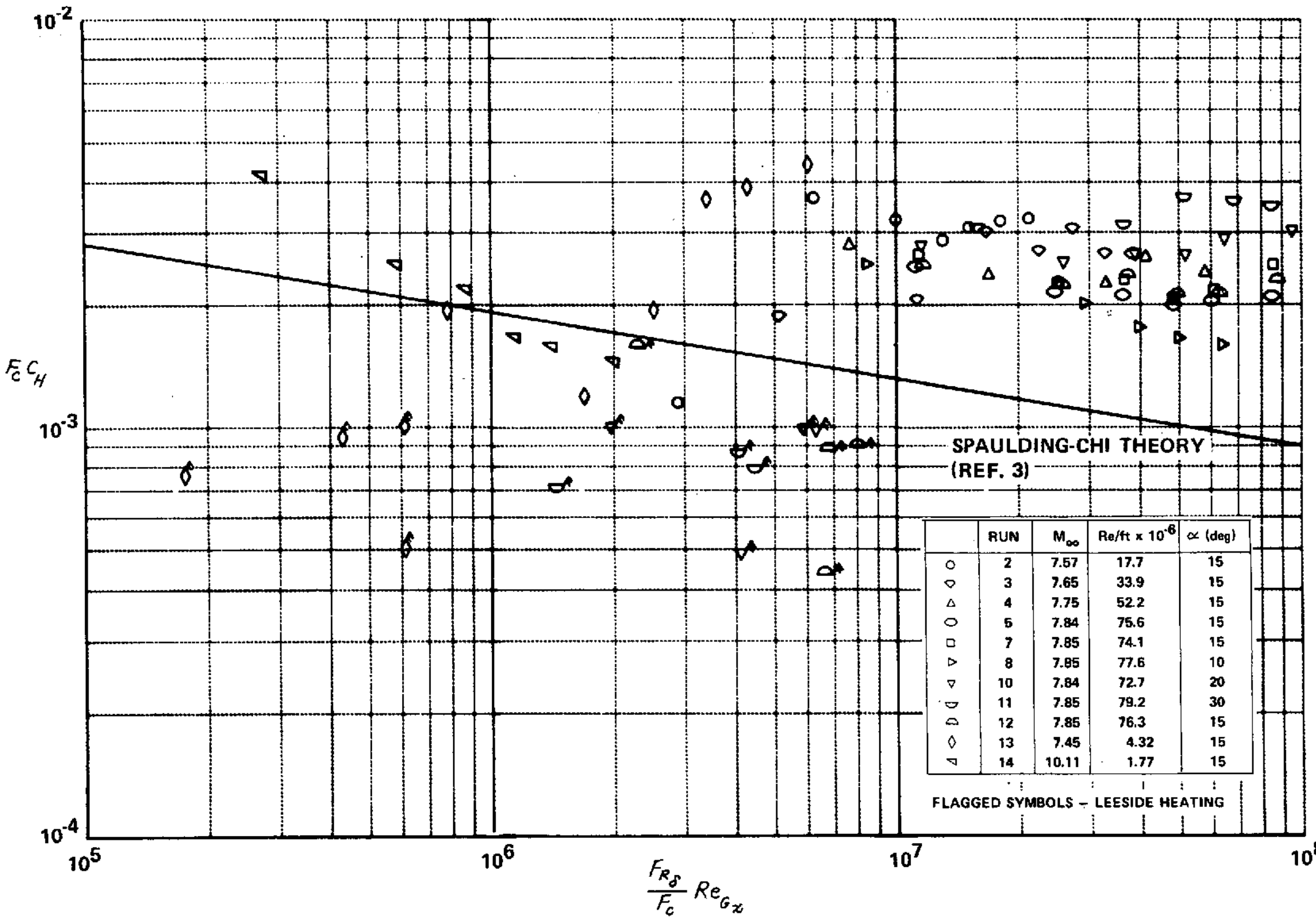

Figure 2 CORRELATION OF WINDWARD AND LEESIDE HEATING WITH TURBULENT BOUNDARY LAYER THEORY

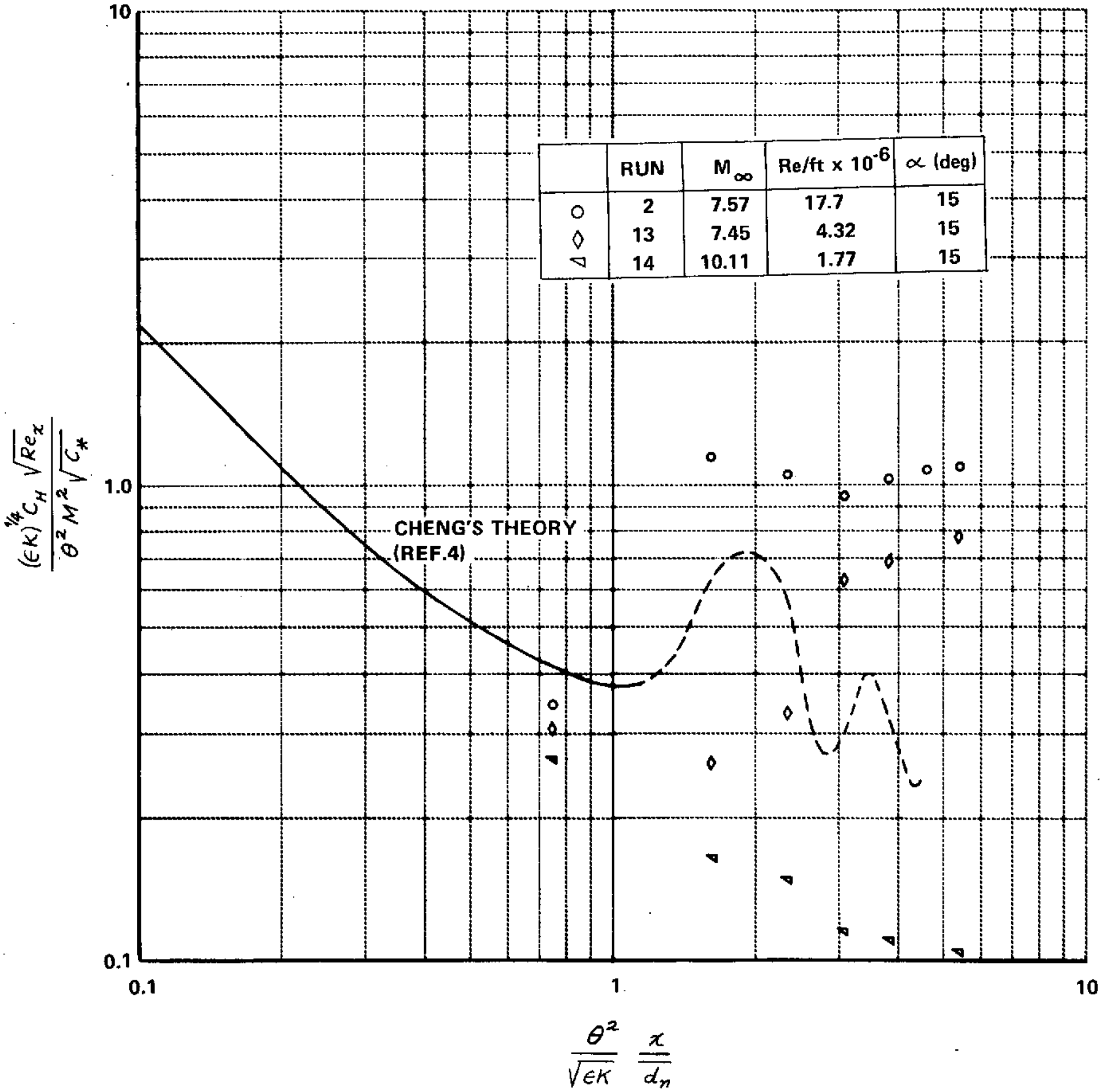

Figure 3 CORRELATION OF WINDWARD HEATING RATES WITH LAMINAR BOUNDARY LAYER THEORY

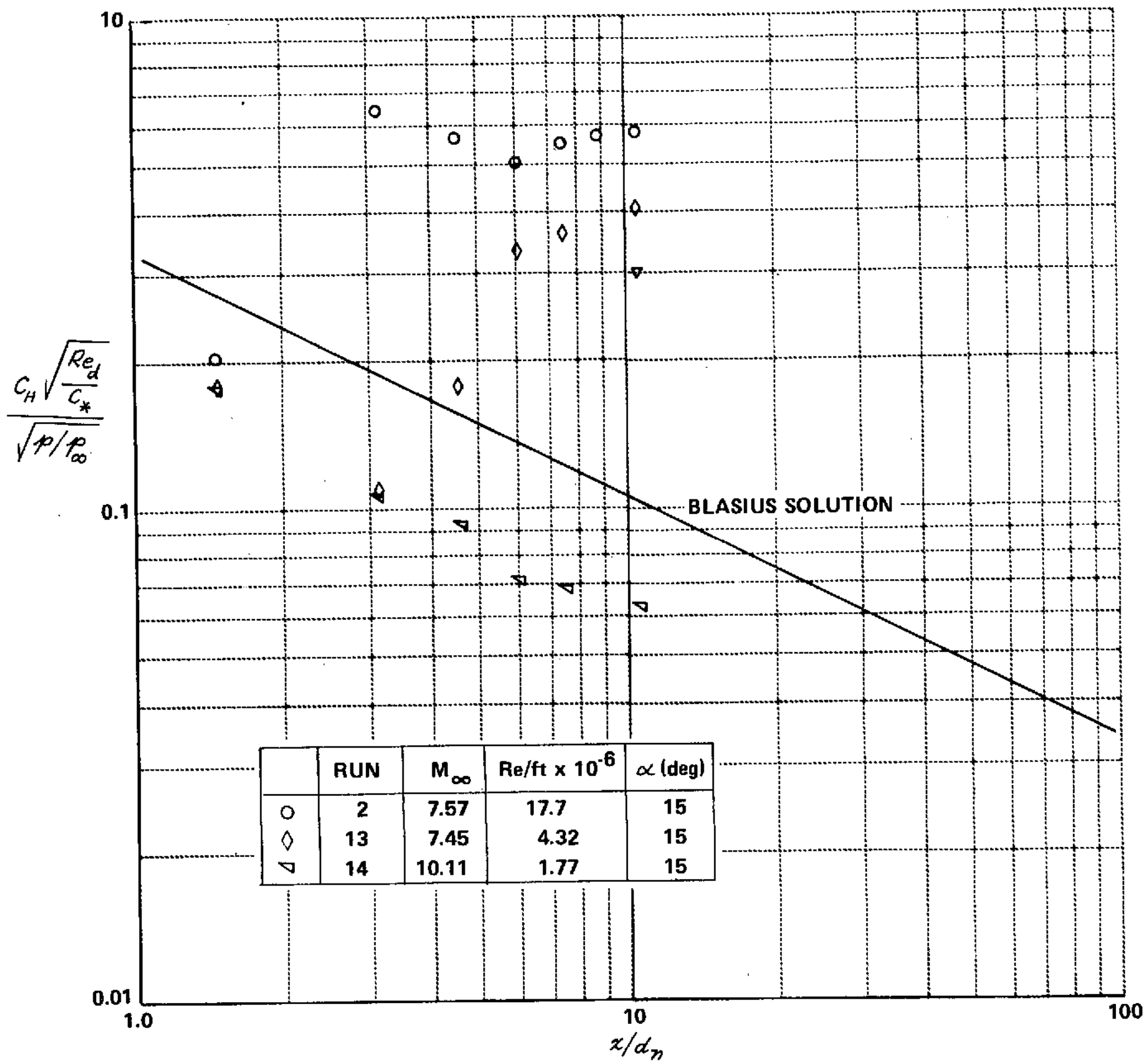

Figure 4 CORRELATION OF WINDWARD HEATING RATES WITH LAMINAR BOUNDARY LAYER THEORY

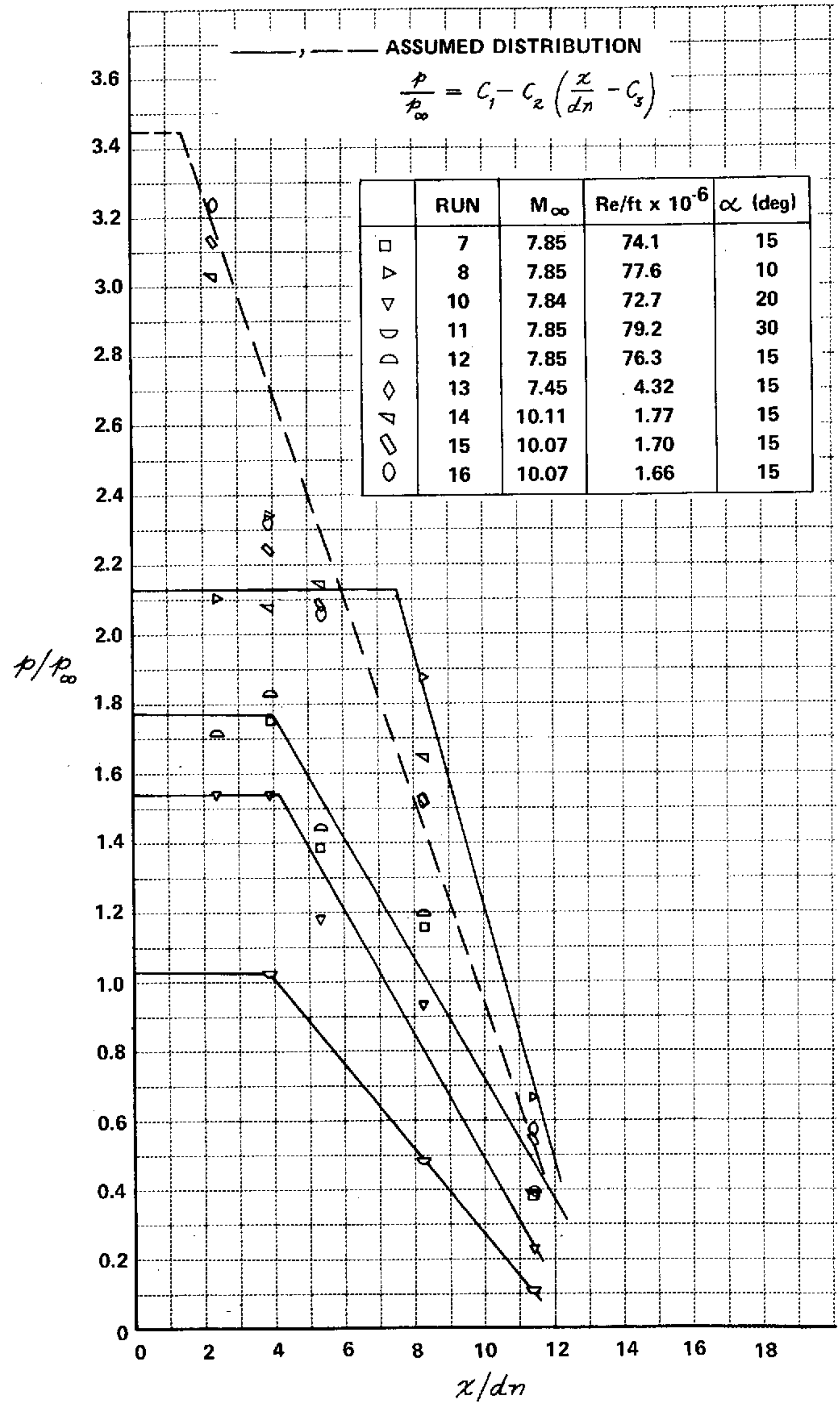

	RUN	M_∞	Re/ft x 10^{-6}	α (deg)
□	7	7.85	74.1	15
▷	8	7.85	77.6	10
▽	10	7.84	72.7	20
D	11	7.85	79.2	30
◠	12	7.85	76.3	15
◇	13	7.45	4.32	15
◁	14	10.11	1.77	15
⬯	15	10.07	1.70	15
○	16	10.07	1.66	15

Figure 5 PRESSURE DISTRIBUTIONS IN THE LEEWARD PLANE OF SYMMETRY

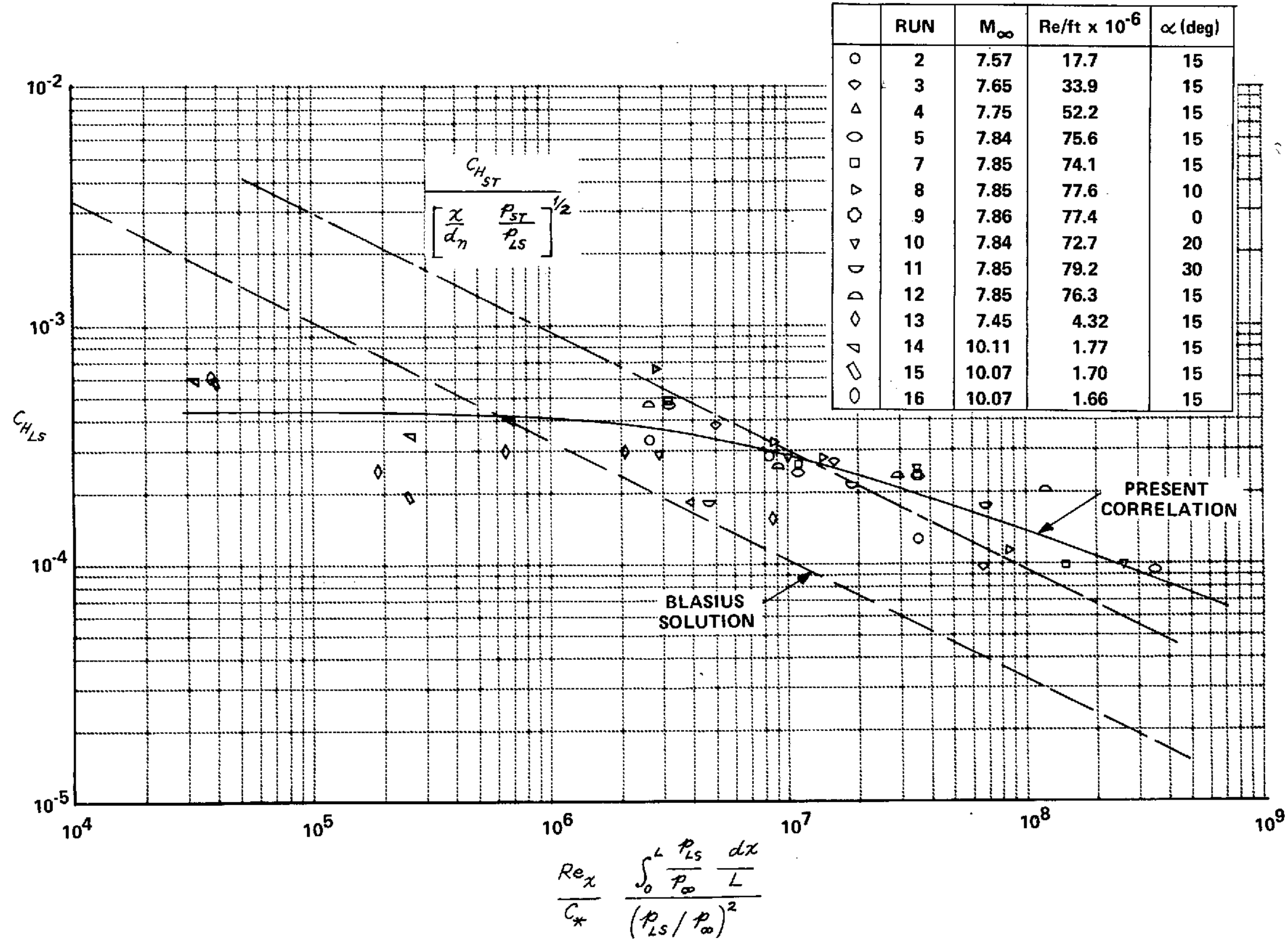

	RUN	M_∞	Re/ft x 10^{-6}	α (deg)
○	2	7.57	17.7	15
◇	3	7.65	33.9	15
△	4	7.75	52.2	15
⬭	5	7.84	75.6	15
□	7	7.85	74.1	15
▷	8	7.85	77.6	10
⬡	9	7.86	77.4	0
▽	10	7.84	72.7	20
◡	11	7.85	79.2	30
◠	12	7.85	76.3	15
◊	13	7.45	4.32	15
◁	14	10.11	1.77	15
⬯	15	10.07	1.70	15
0	16	10.07	1.66	15

Figure 6 CORRELATION OF LEESIDE HEATING RATES